In-Space Electric Propulsion Applications

Wake Aligned Repeating Pulse System x2 30kW pods, 1 PORT, 1 STBD

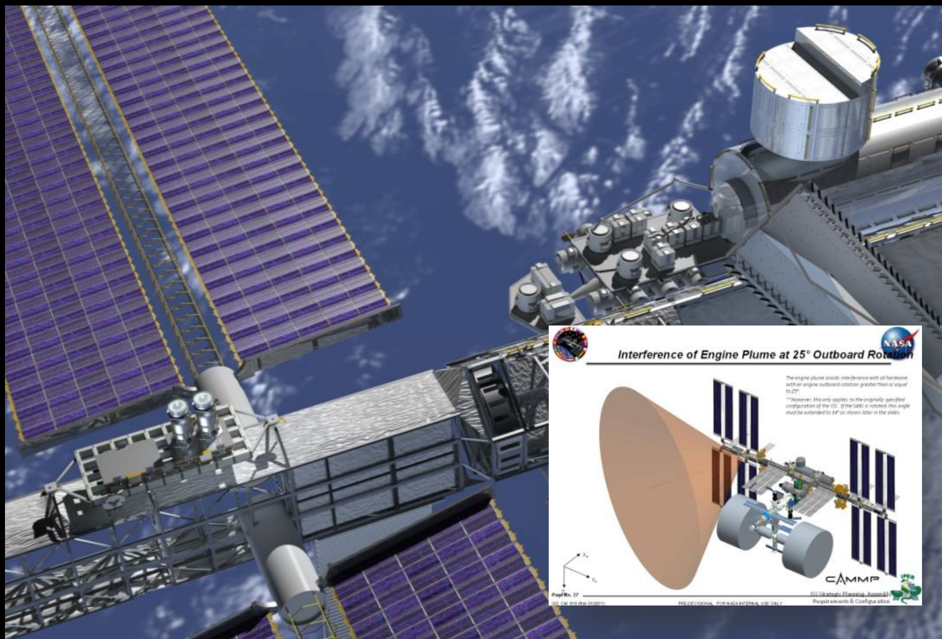

ISS EP&P Free-Flyer Testbed

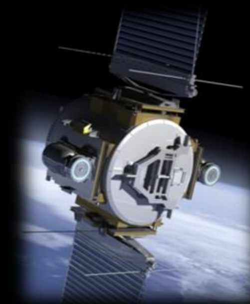

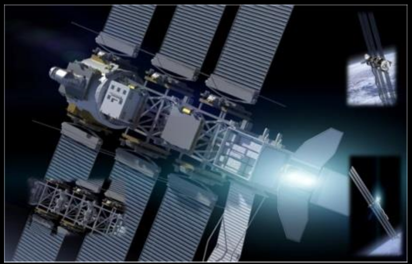

ISS EP&P Static Testbed

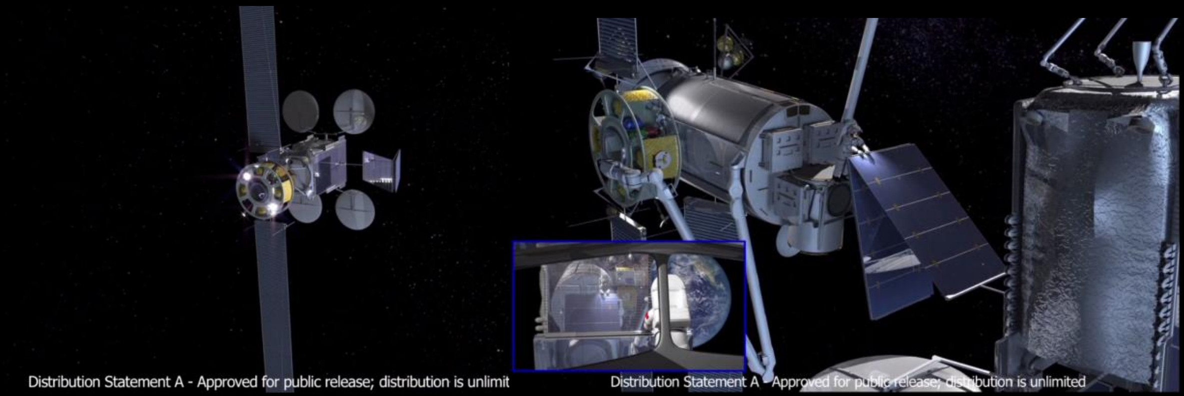

NASA-DARPA 30kW tug concept supporting Manned Geosynchronous Satellite Servicing Architecture

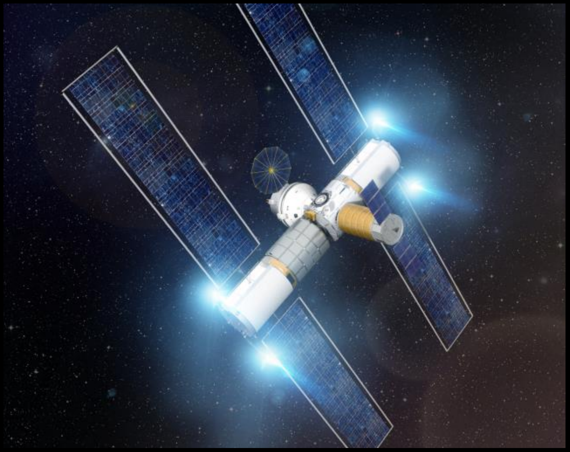

Waypoint/Gateway

Eagleworks Laboratories
Advanced Propulsion

Dr. Harold "Sonny" White
NASA JSC

Picture courtesy of NASA,
http://www.nasa.gov/centers/glenn/technology/warp/warpstat.html

ACT I: Space Warps

The Challenge of Interstellar Flight

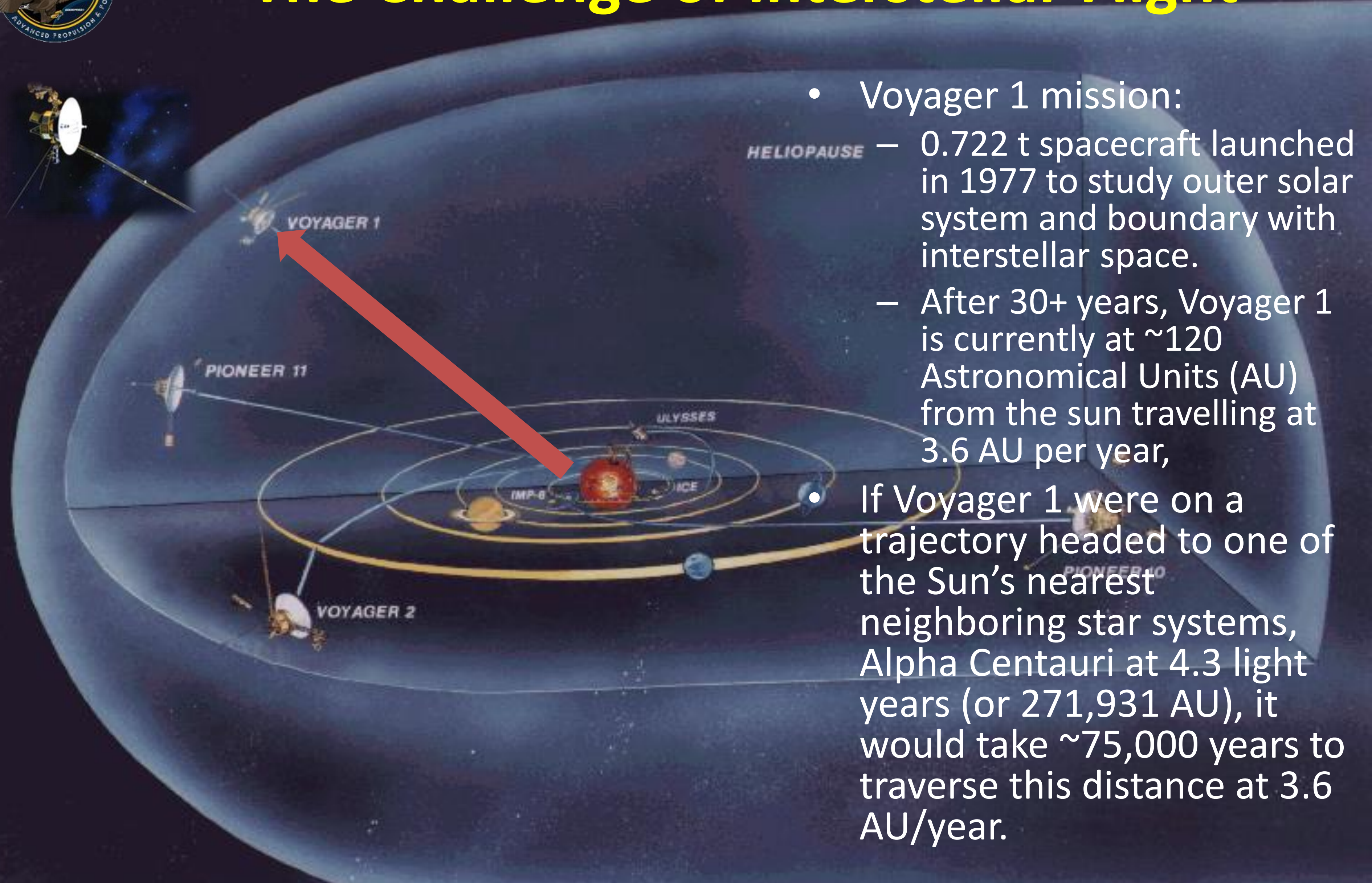

- Voyager 1 mission:
  - 0.722 t spacecraft launched in 1977 to study outer solar system and boundary with interstellar space.
  - After 30+ years, Voyager 1 is currently at ~120 Astronomical Units (AU) from the sun travelling at 3.6 AU per year,
- If Voyager 1 were on a trajectory headed to one of the Sun's nearest neighboring star systems, Alpha Centauri at 4.3 light years (or 271,931 AU), it would take ~75,000 years to traverse this distance at 3.6 AU/year.

Pictures courtesy of NASA,
http://voyager.jpl.nasa.gov/imagesvideo/images/voyager2_large.jpg
http://voyager.jpl.nasa.gov/mission/interstellar.html

DAEDELUS

- **Project Daedelus sponsored by British Interplanetary Society in 1970’s to develop robotic interstellar probe capable of reaching Barnard’s star, at ~6 light years away, in 50 years.**
- **The resulting spacecraft was 54,000t,**
- **92% fuel for fusion propulsion system.**
- **ISS is ~450t**

Picture courtesy of Adrian Mann, www.bisbos.com, used with permission
ISS picture courtesy of NASA (STS-135 fly-around)


IS THERE ANOTHER WAY??

Hyper-fast interstellar travel…

- Is there a way within the framework of physics such that one could cross any given cosmic distance in an arbitrarily short period of time, while never locally breaking the speed of light (11th commandment)?

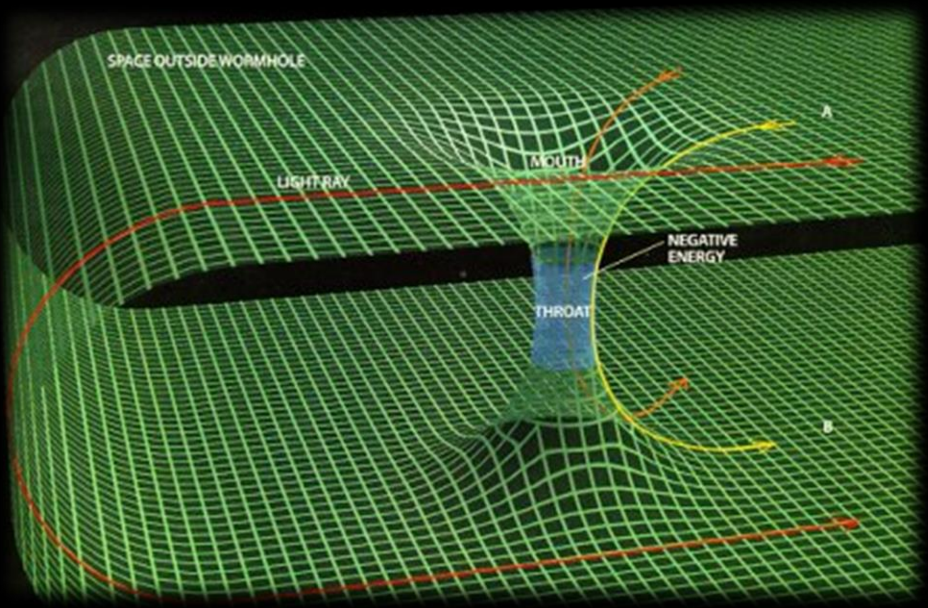

WORMHOLES (shortcuts)

SPACEWARPS (inflation)

Images courtesy NASA

Inflation: Alcubierre Metric[1]

Warp Metric:

$$ds^2 = -dt^2 + (dx - v_s f(r_s)dt)^2 + dy^2 + dz^2$$

Apparent speed (↑ v_s)

Shaping Function:

Shell thickness parameter (σ) — Shell size parameter (R)

$$f(r_s) = \frac{\tanh(\sigma(r_s + R)) - \tanh(\sigma(r_s - R))}{2\tanh(\sigma R)}$$

York Time:

$$\theta = v_s \frac{x_s}{r_s} \frac{df(r_s)}{dr_s}$$

York Time is measure of expansion/contraction of space

Energy Density:

$$\frac{1}{8\pi} G^{00} = -\frac{1}{8\pi} \frac{v_s^2 (y^2 + z^2)}{4 r_s^2} \left(\frac{df(r_s)}{dr_s} \right)^2$$

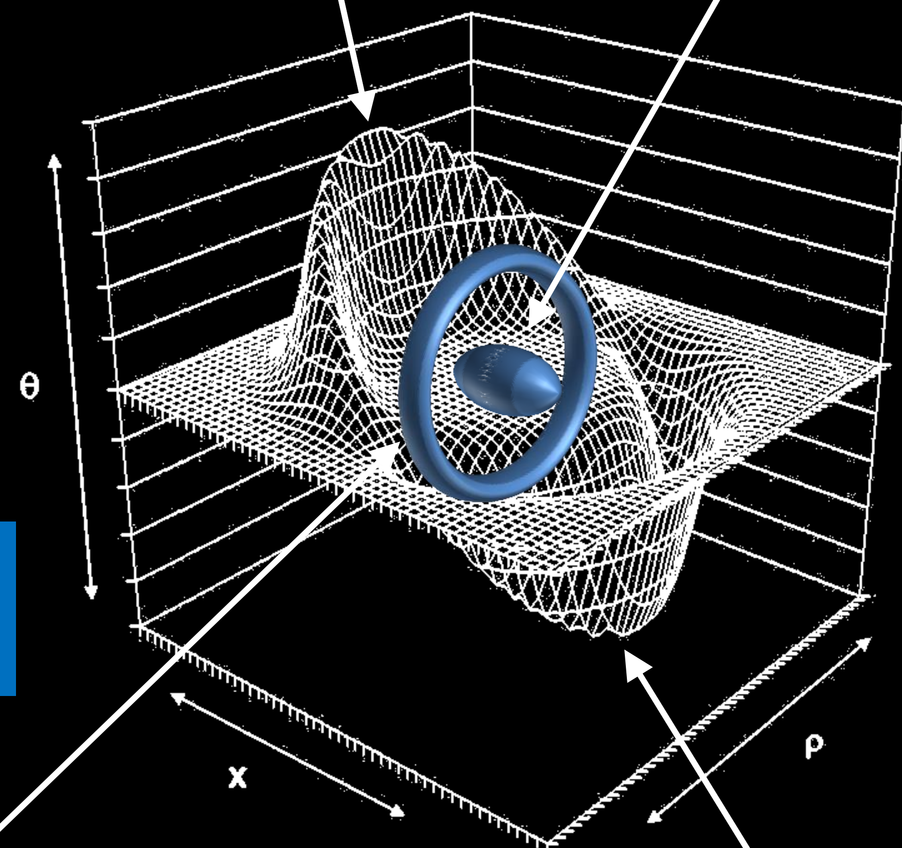

1. Alcubierre, M., "The warp drive: hyper-fast travel within general relativity," Class. Quant. Grav. 11, L73-L77 (1994).

Appealing Characteristics

Proper acceleration in the bubble is formally zero

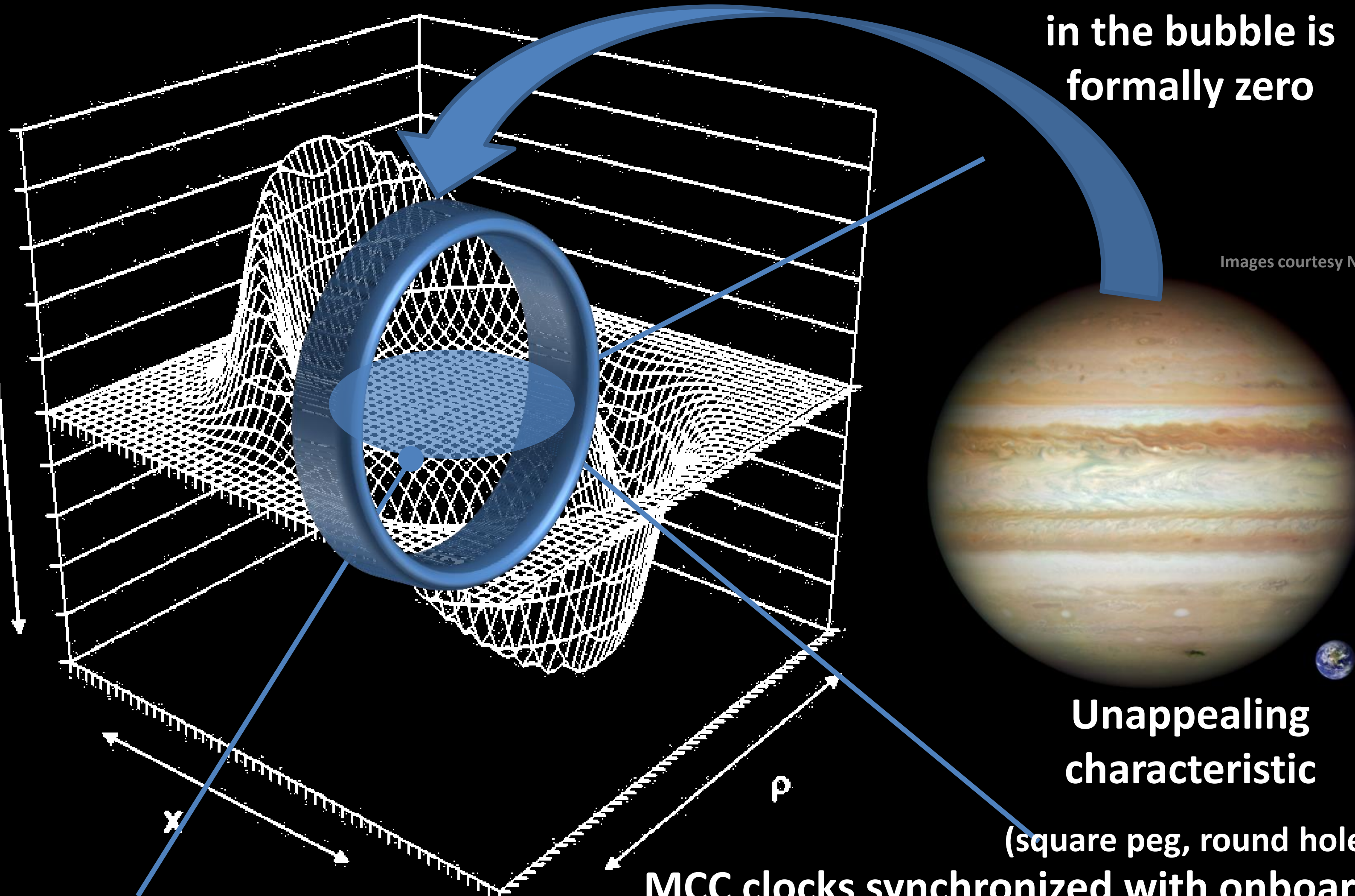

Unappealing characteristic

(square peg, round hole)

MCC clocks synchronized with onboard clocks

(Coordinate time = proper time)

Flat space-time inside the bubble

(divergence of phi = 0)

Bubble Topology Optimization

York Time magnitude decreases

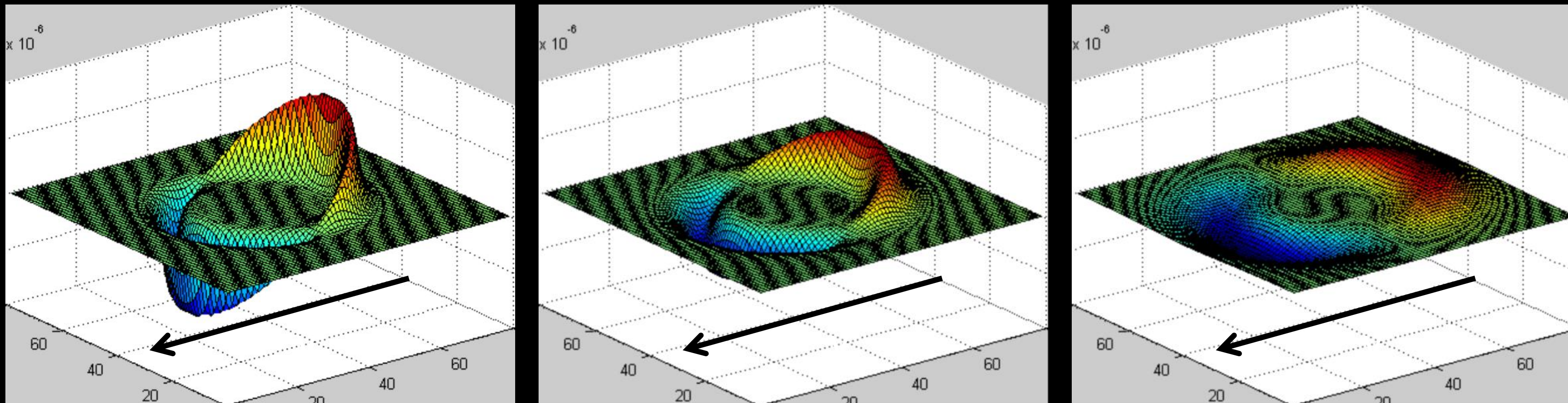

"bubble" thickness decreases

Energy density magnitude decreases

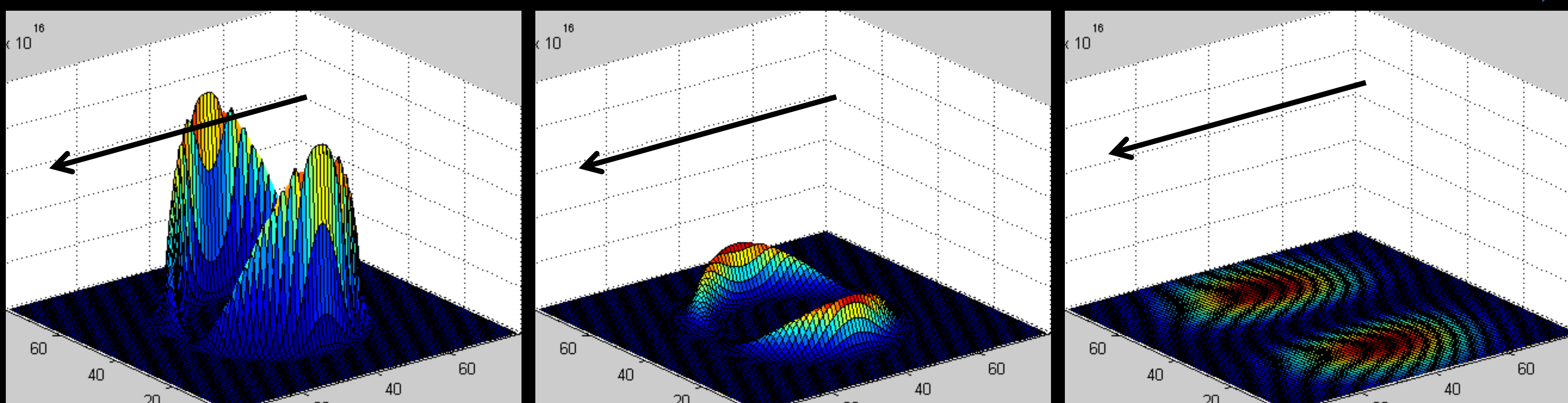

"bubble" thickness decreases

Surface plots of York Time & T^{00}, <v>=10c, 10 meter diameter volume, variable warp "bubble" thickness

As bubble thickness increases, York Time intensity decreases

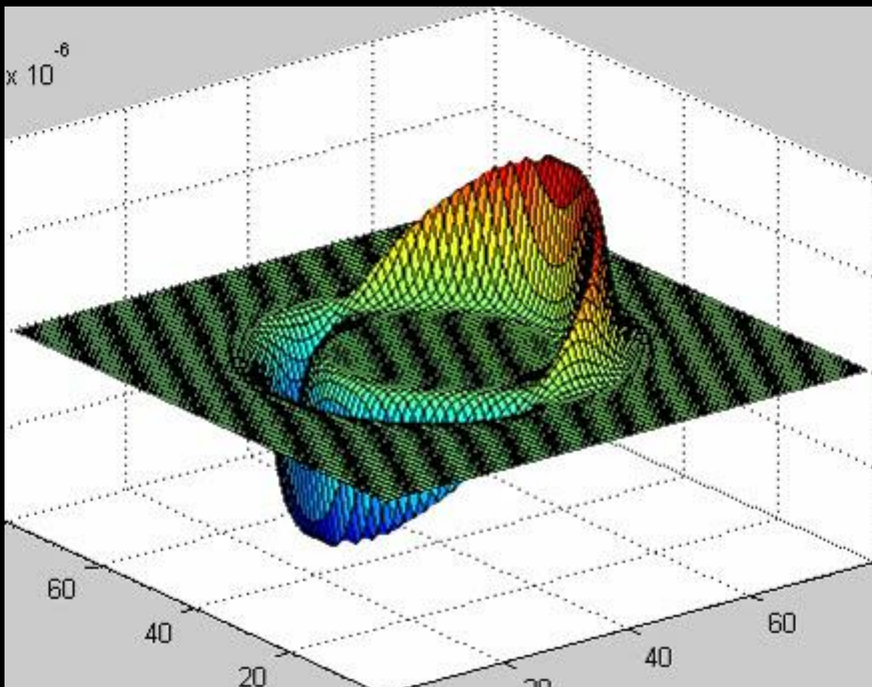

Allowing the bubble to get thicker reduces the flat space-time real-estate in the center

Changing topology greatly reduces the energy required

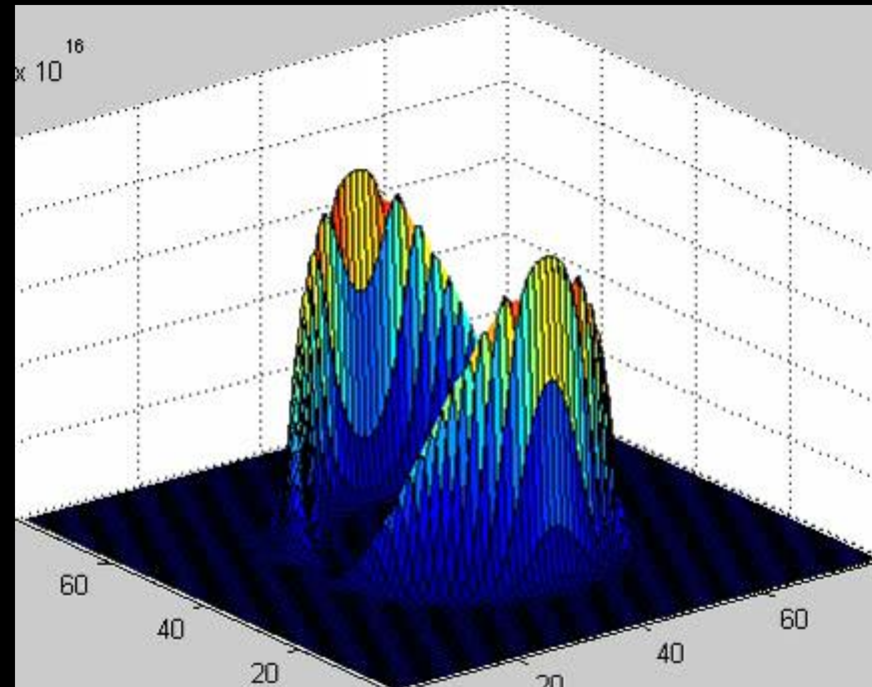

But space-time is really stiff: $c^4/8\pi G$

Can we further reduce the energy required by reducing the stiffness?

<u>Maybe…</u>but we need to engage higher dimensional models to do so

Bubble Oscillation Optimization

$$ds^2 = -c^2dt^2 + \frac{a^2(t)}{e^{2kU}}dX^2 + dU^2$$

$$\frac{dX}{dt} = \frac{ce^{kU}}{a(t)}\sqrt{1-\frac{dU^2}{c^2dt^2}}$$

$$\frac{dU}{dt} \Rightarrow 1, U = 0 \quad \therefore \frac{dX}{dt} \Rightarrow 0$$

$$\gamma \approx e^U \quad \phi \approx U \quad \frac{d\phi}{dt} \approx \frac{dU}{dt}$$

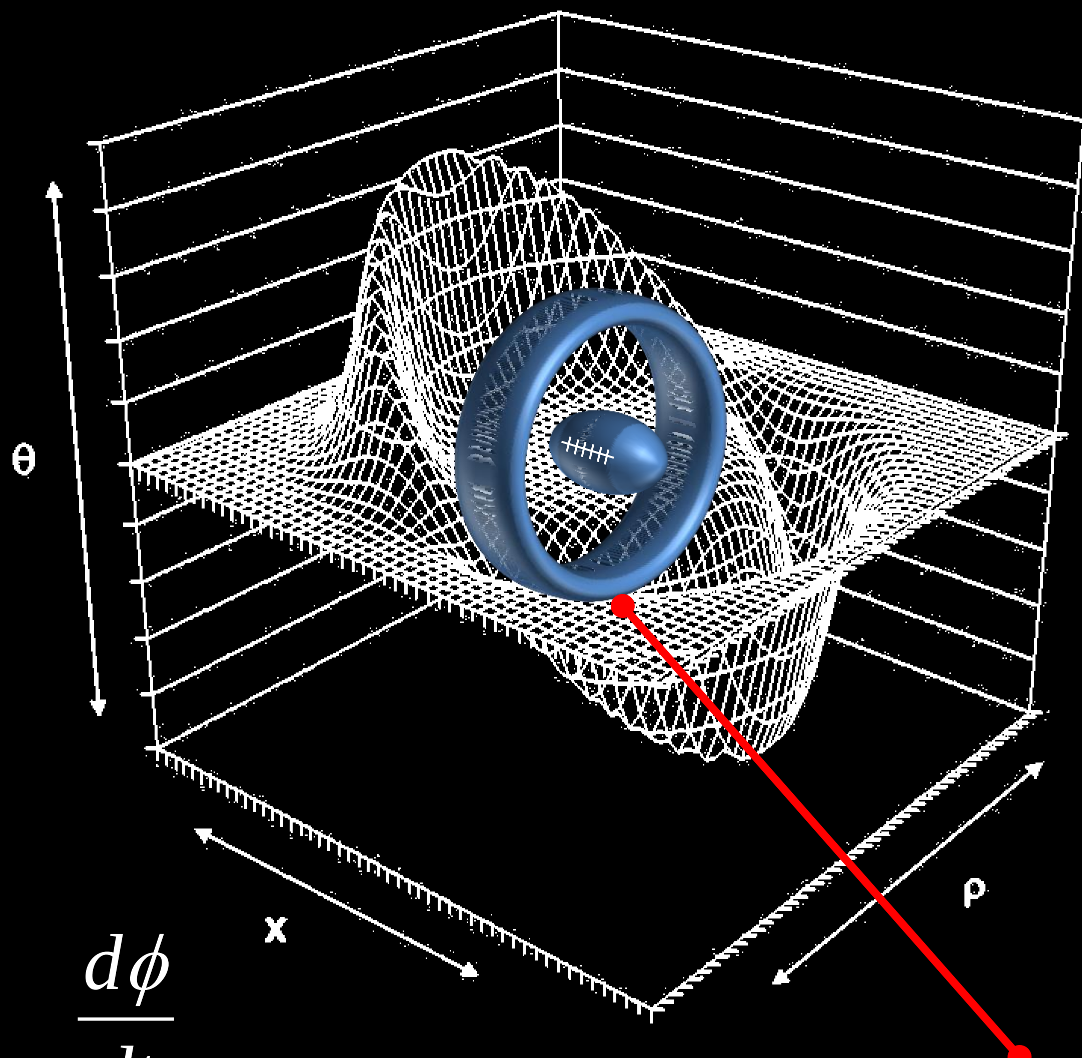

$$\frac{d\phi}{dt}$$

Oscillate the bubble intensity

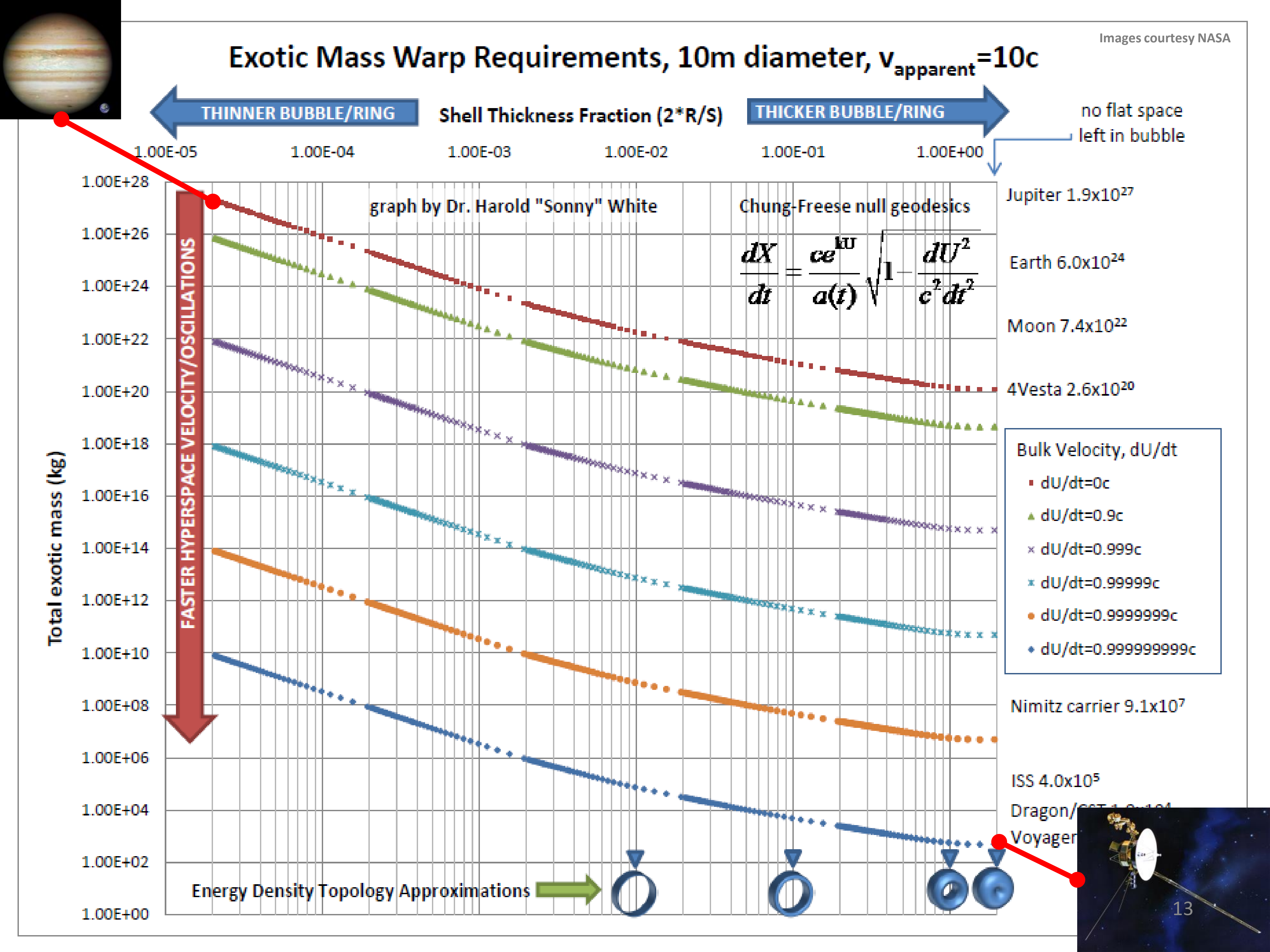
Images courtesy NASA
Exotic Mass Warp Requirements, 10m diameter, v_apparent=10c
THINNER BUBBLE/RING
Shell Thickness Fraction (2*R/S)
THICKER BUBBLE/RING
no flat space left in bubble
1.00E-05
1.00E-04
1.00E-03
1.00E-02
1.00E-01
1.00E+00
1.00E+28
1.00E+26
1.00E+24
1.00E+22
1.00E+20
1.00E+18
1.00E+16
1.00E+14
1.00E+12
1.00E+10
1.00E+08
1.00E+06
1.00E+04
1.00E+02
1.00E+00
Total exotic mass (kg)
FASTER HYPERSPACE VELOCITY/OSCILLATIONS
graph by Dr. Harold "Sonny" White
Chung-Freese null geodesics
$$\frac{dX}{dt} = \frac{ce^{kU}}{a(t)}\sqrt{1 - \frac{dU^2}{c^2 dt^2}}$$
Jupiter 1.9x10^27
Earth 6.0x10^24
Moon 7.4x10^22
4Vesta 2.6x10^20
Bulk Velocity, dU/dt
dU/dt=0c
dU/dt=0.9c
dU/dt=0.999c
dU/dt=0.99999c
dU/dt=0.9999999c
dU/dt=0.999999999c
Nimitz carrier 9.1x10^7
ISS 4.0x10^5
Dragon/
Voyager
Energy Density Topology Approximations

Warp Field Interferometer

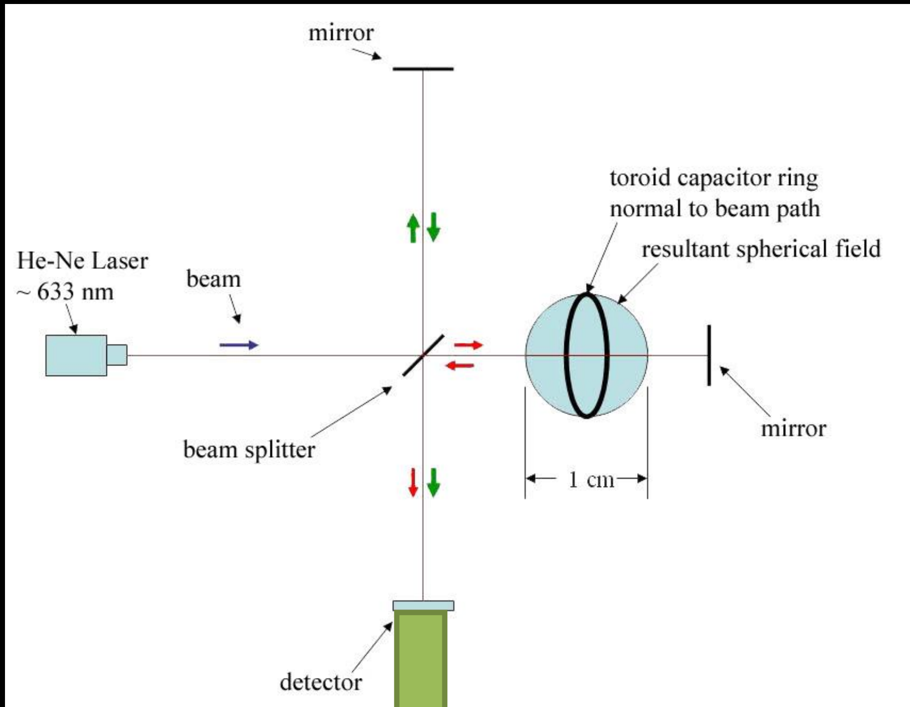

- Warp Field Interferometer developed after putting metric into canonical form[1]:

$$ds^2 = (v_s^2 f(r_s)^2 - 1)\left\{dt - \frac{v_s f(r_s)}{v_s^2 f(r_s)^2 - 1}dx\right\}^2 - dx^2 + dy^2 + dz^2$$

- Generate microscopic warp bubble that perturbs optical index by 1 part in 10,000,000
- Induce relative phase shift between split beams that should be detectable.

$X(x,y)$

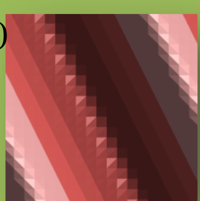

Numerical simulation of fringe at detector with device off

$X_1(x,y)$

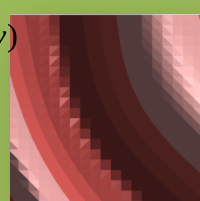

Numerical simulation of fringe at detector with device on

2D Analytic Signal processing

$M(x,y)e^{j\phi(x,y)}$

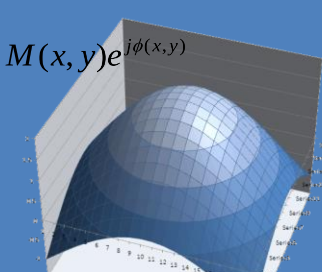

Numerical simulation of contour plot of ϕ for warp field

1. White, H., "A Discussion on space-time metric engineering," Gen. Rel. Grav. 35, 2025-2033 (2003).

Interferometer and Test-article Setup

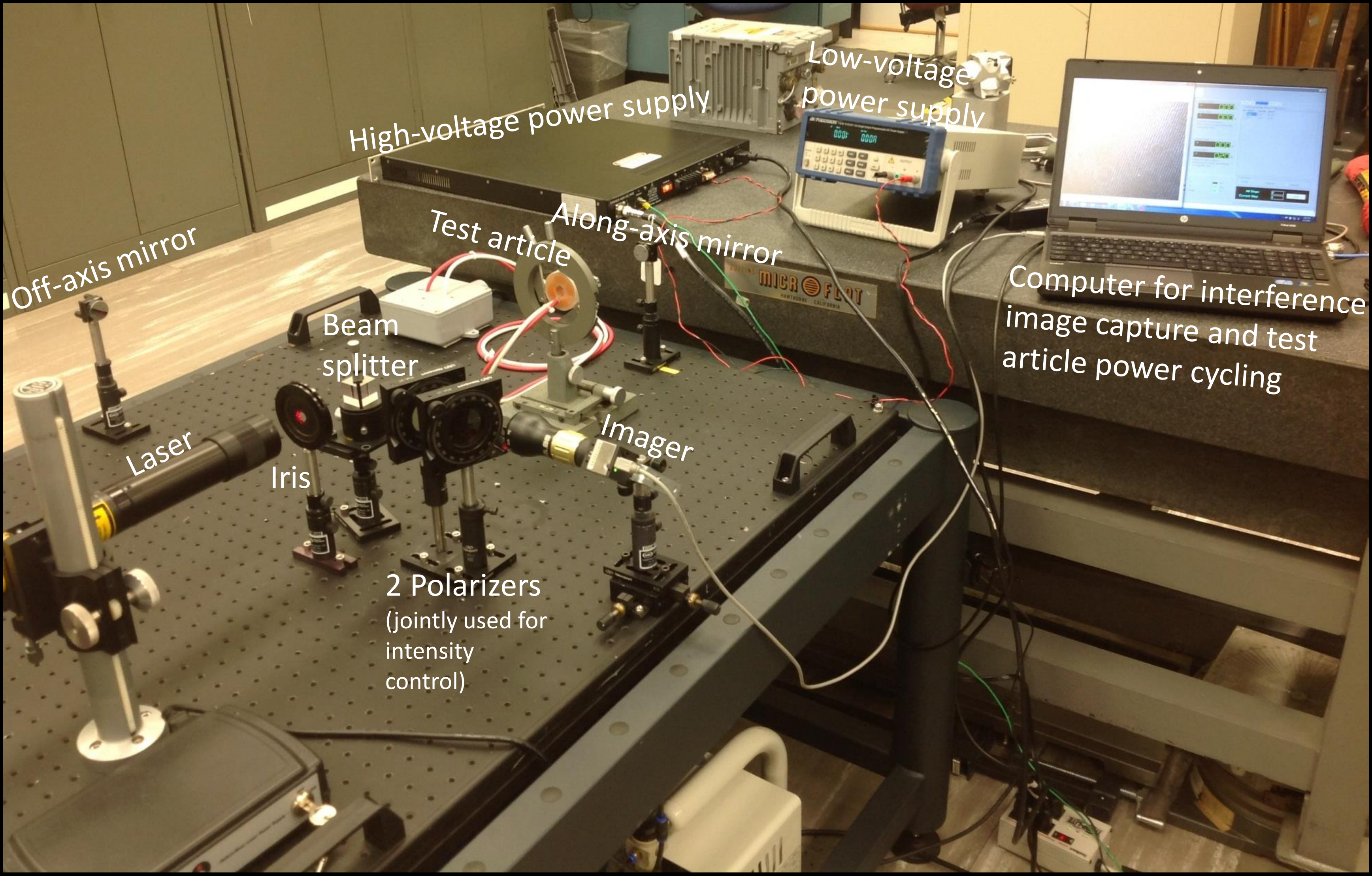

Fabry-Perot Interferometer

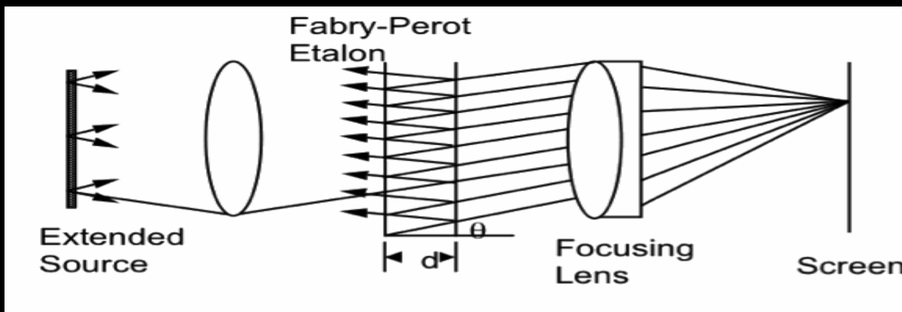

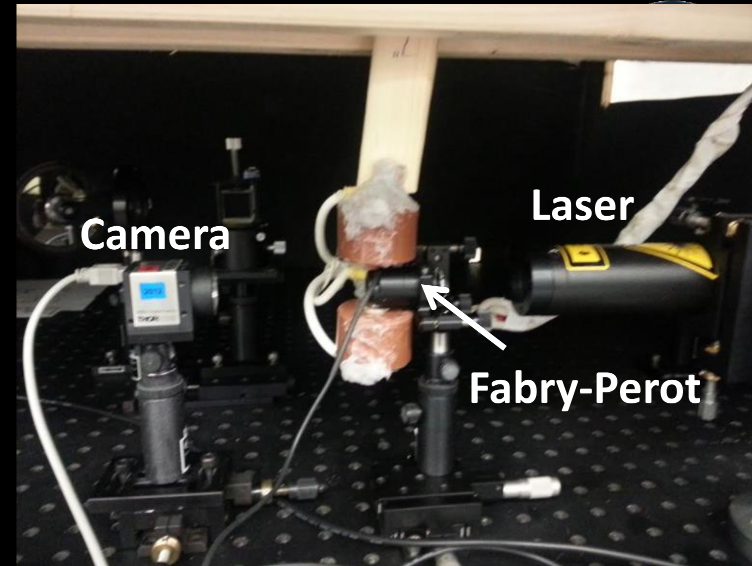

Example: Michelson-Morley Interferometer image for Sodium source

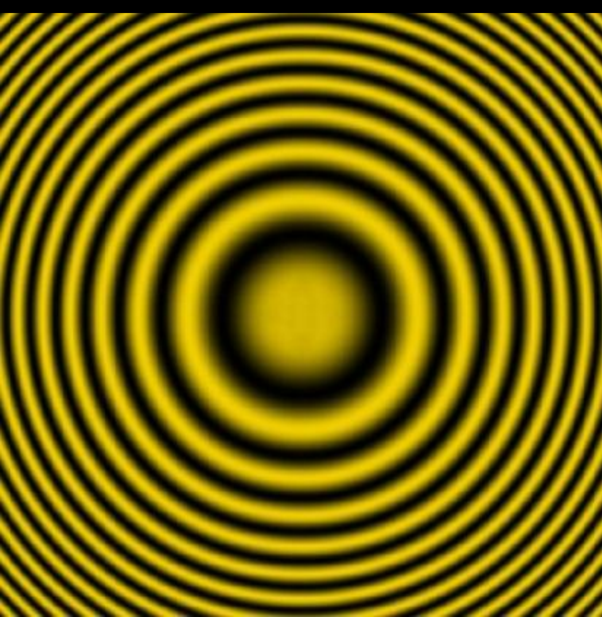

- Consists of two reflecting, highly parallel surfaces, called an Etalon
- The interference pattern is created within the Etalon
- Multiple reflections in the Etalon reinforce the areas where constructive and destructive interference occurs
- Allows for much higher-precision measurements of fringes (image averaging without software)

Example: Fabry-Perot Interferometer image for Sodium source (note doublet)

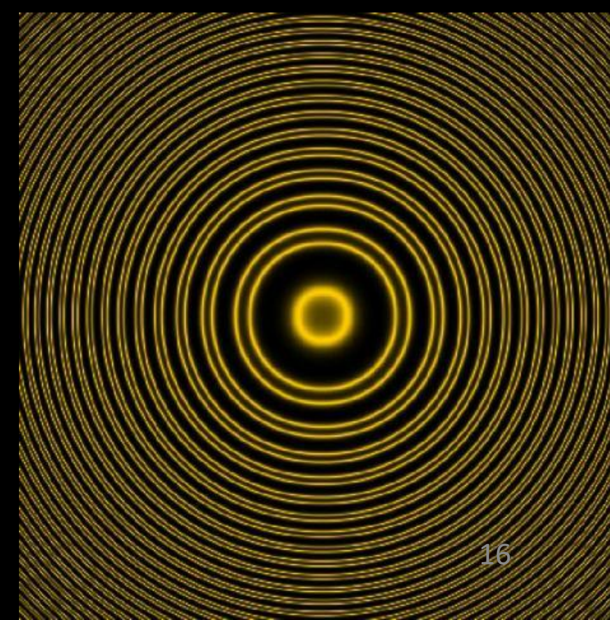

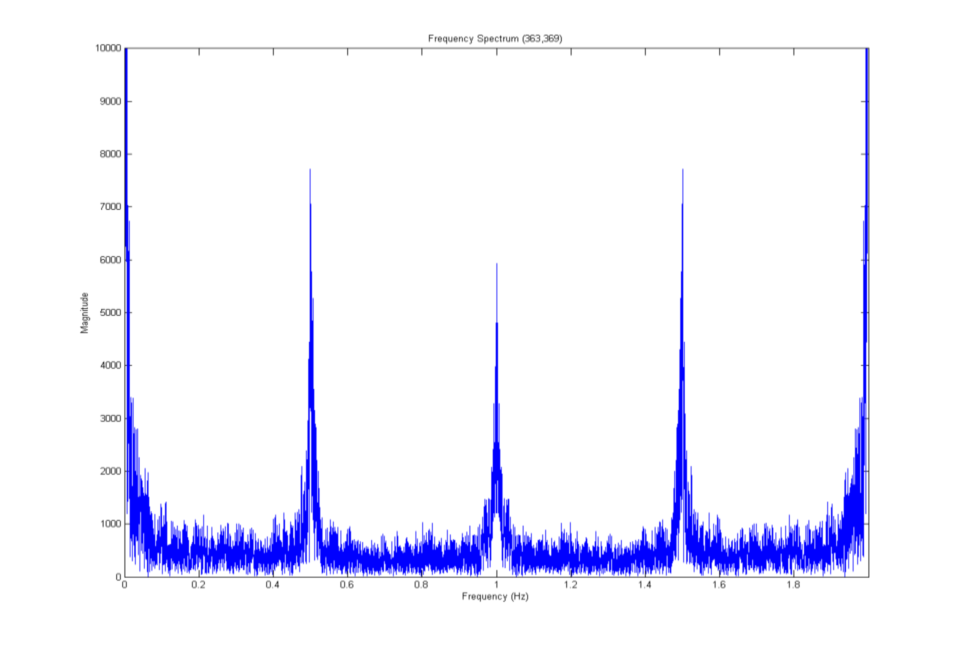

FFT of single pixel

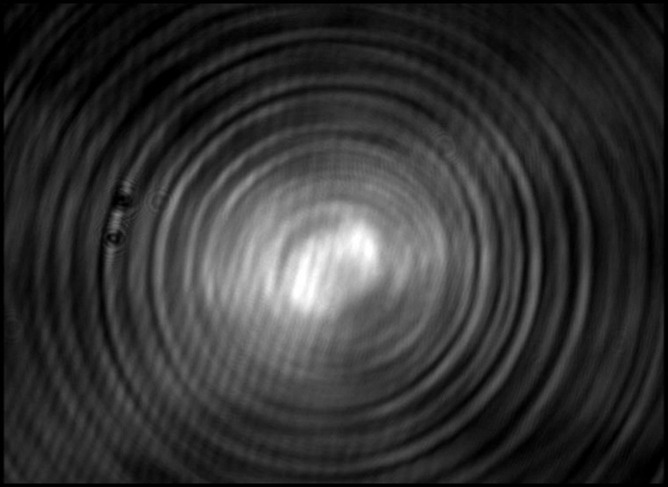

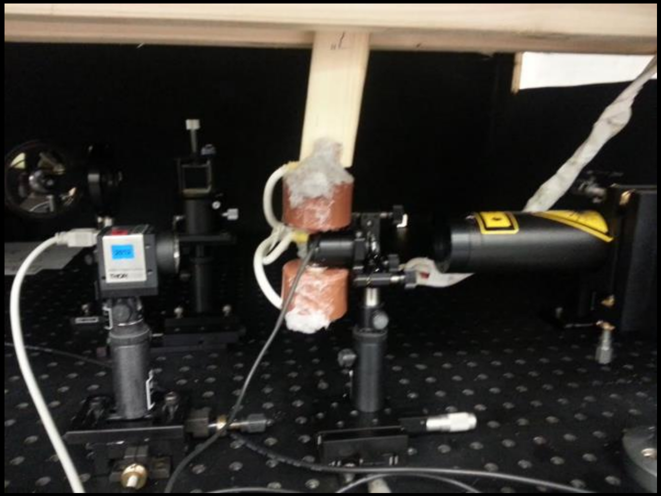

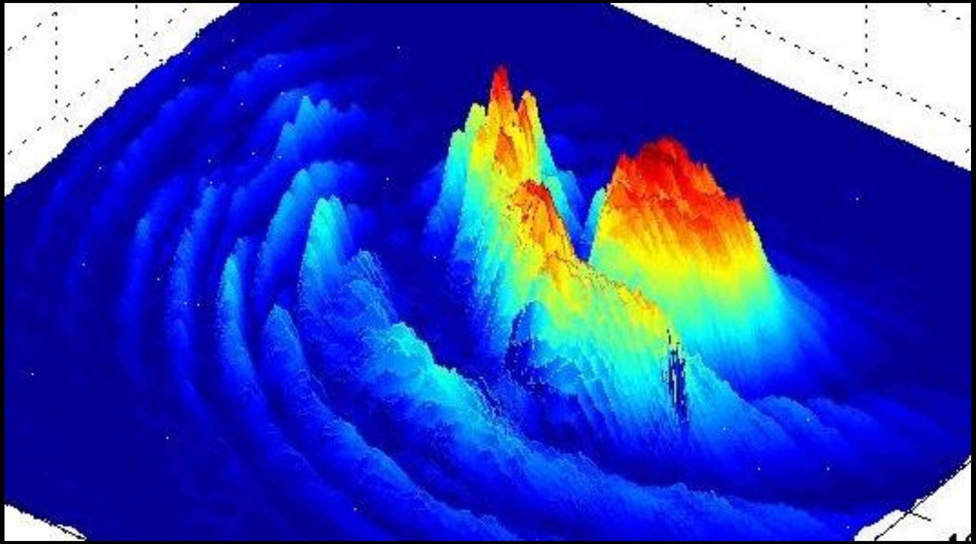

FFT of entire imager at frequency of interest

Isolated Lab

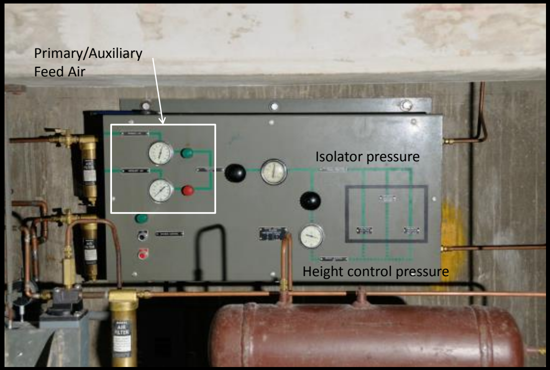

FFT of imager data at frequency of interest

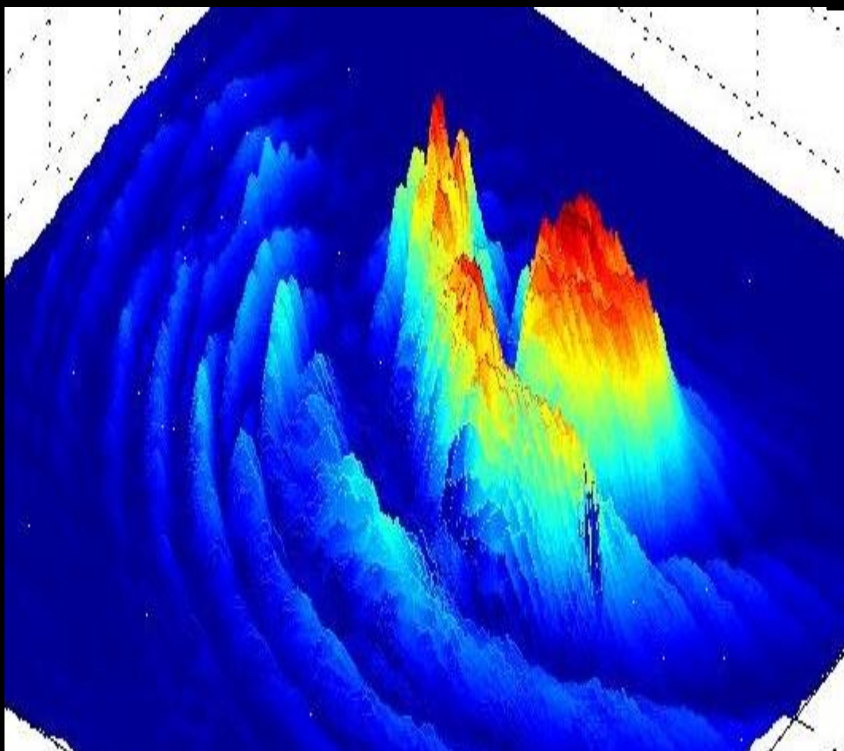

isolated

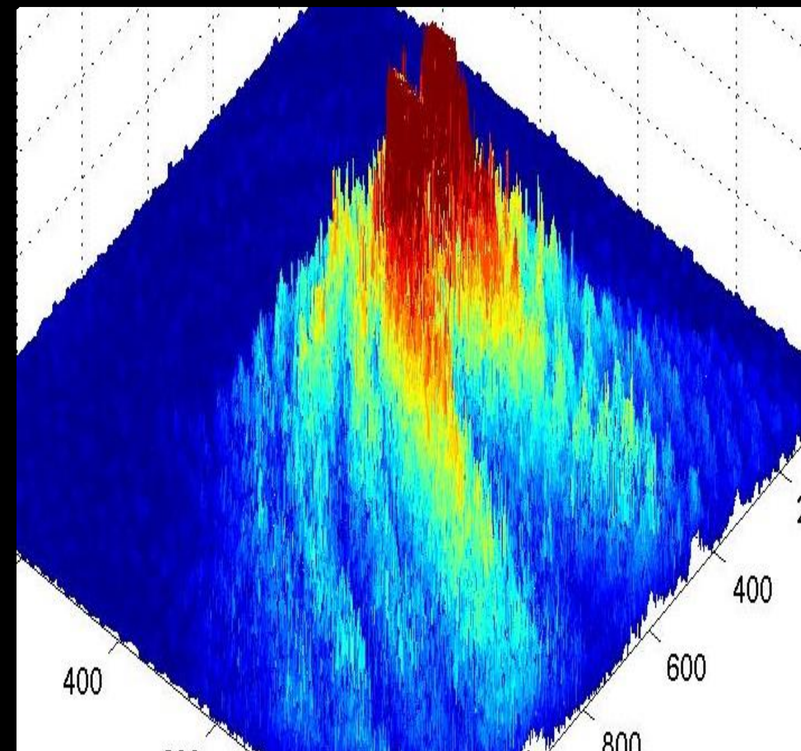

not isolated

Open-air etalon Implementation

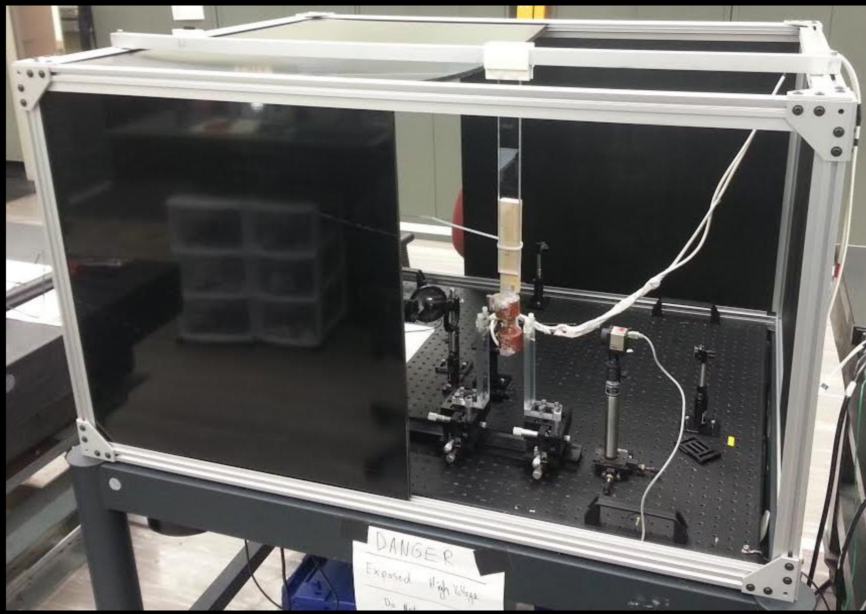

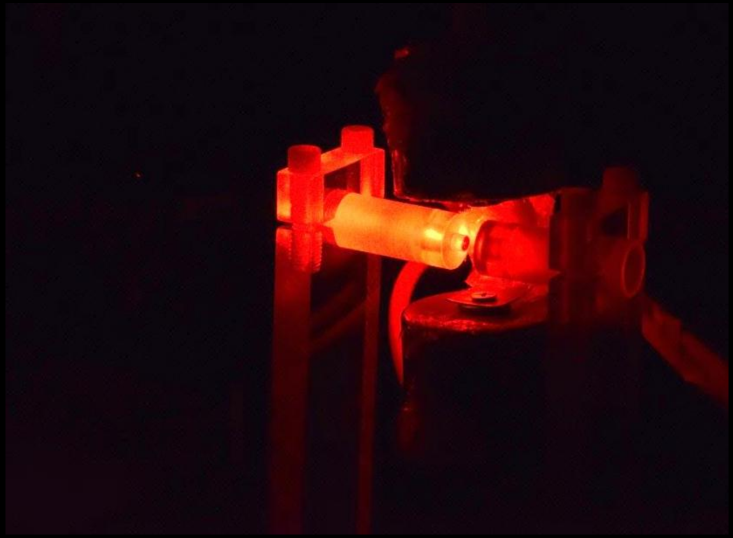

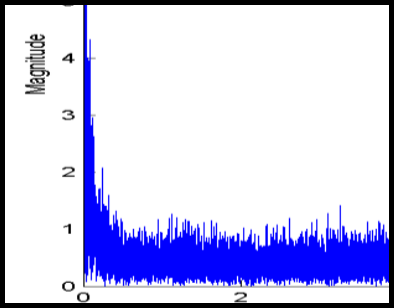

Inactive

Frequencies of interest

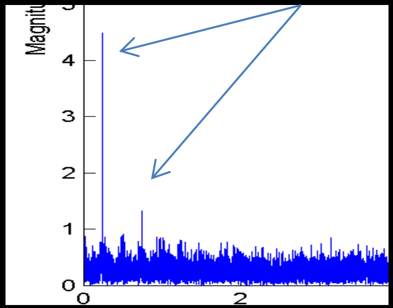

Active

Time of Flight Schematic

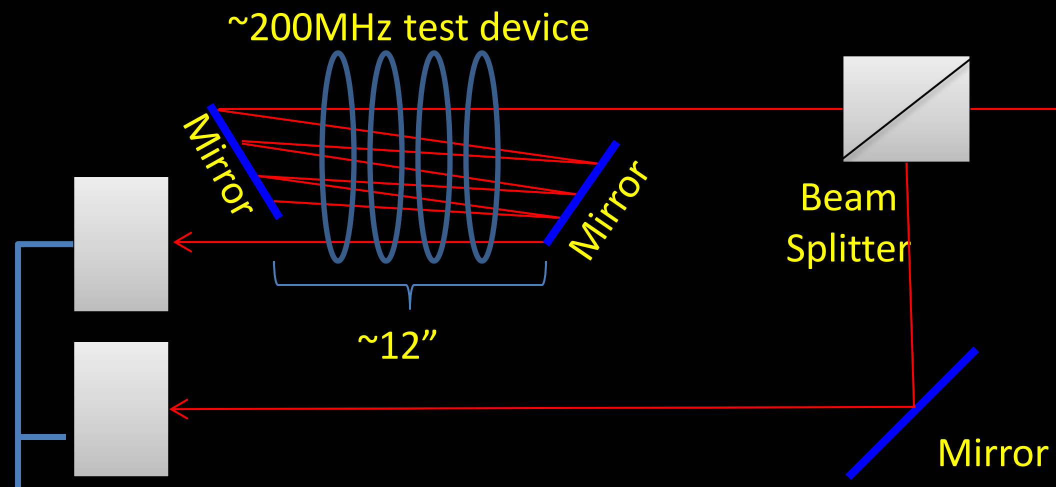

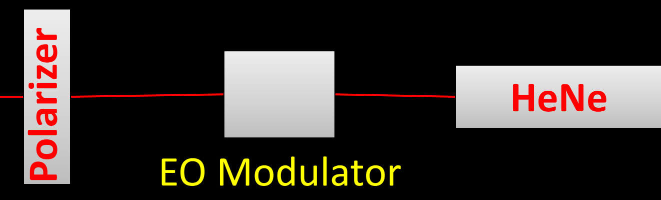

Newport Broadband Amplitude Modulator

Model	4102NF
Type	Broadband Amplitude Modulator
Operating Frequency	DC-200 MHz
Wavelength Range	500-900 nm
Material	$MgO:LiNbO_3$
Maximum Vπ	195 V @ 633 nm
Maximum Input Power	2 W/mm^2 @ 532 nm
Aperture Diameter	2 mm
RF Bandwidth	200 MHz
RF Connector	SMA
Input Impedance	10 pF
Maximum RF Power	10 W
Connector	SMA

Thorlabs High-Speed Avalanche Detector

Model	APD210
Rise Time	0.5 ns
Supply Voltage	+12 to +15 V
Current Consumption	200 mA
Max. Incident Power	10 mW
Spectral Range	400 – 1000 nm
Frequency Range	1-1600 mHz
Maximum Gain	2.5x10^5 V/W

Agilent Technologies Infiniium DSO9254A 2.5 GHz Oscilloscope

- 2.5 GHz bandwidth across all 4 analog channels
- 20 GSa/s max. sample rate
- Standard 20 Mpts memory per channel, upgradeable to 1 Gpts

Forward Plan

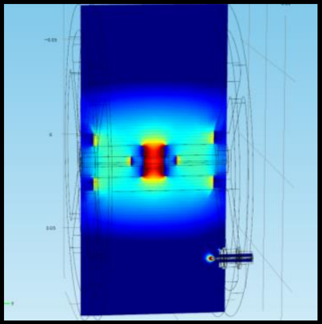

- Explore the $d\phi/dt$ dependency in future test devices
  - The idea of an optimized space warp needs vacuum energy, and large $d\phi/dt$
  - both of these conditions are predicted to be present in the q-thruster technology also being explored in the lab.

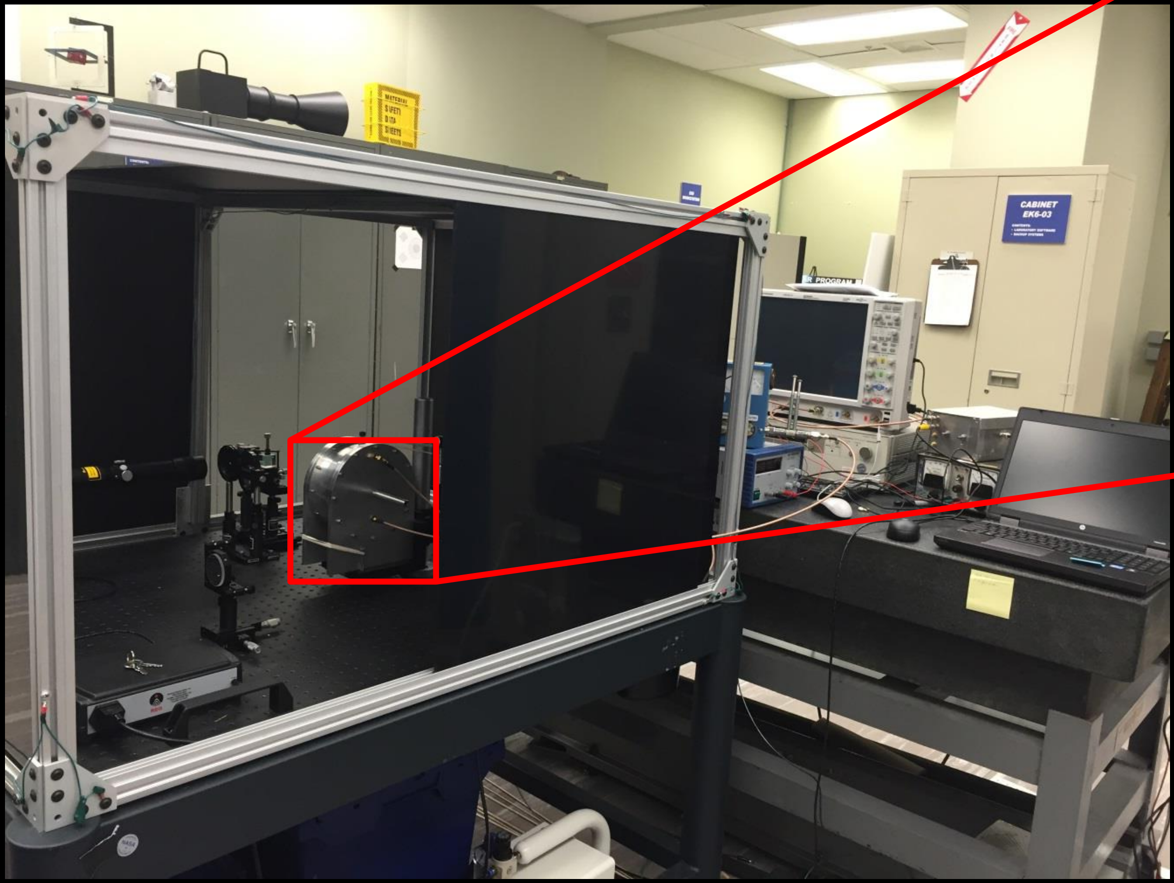

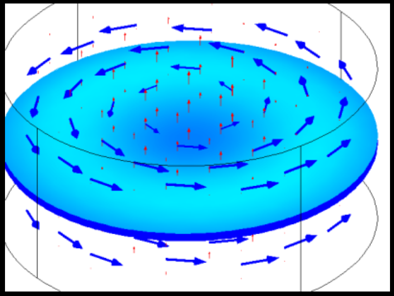

TM010

Original Matthew Jeffries concept from mid 1960's, rendered by Mark Rademaker

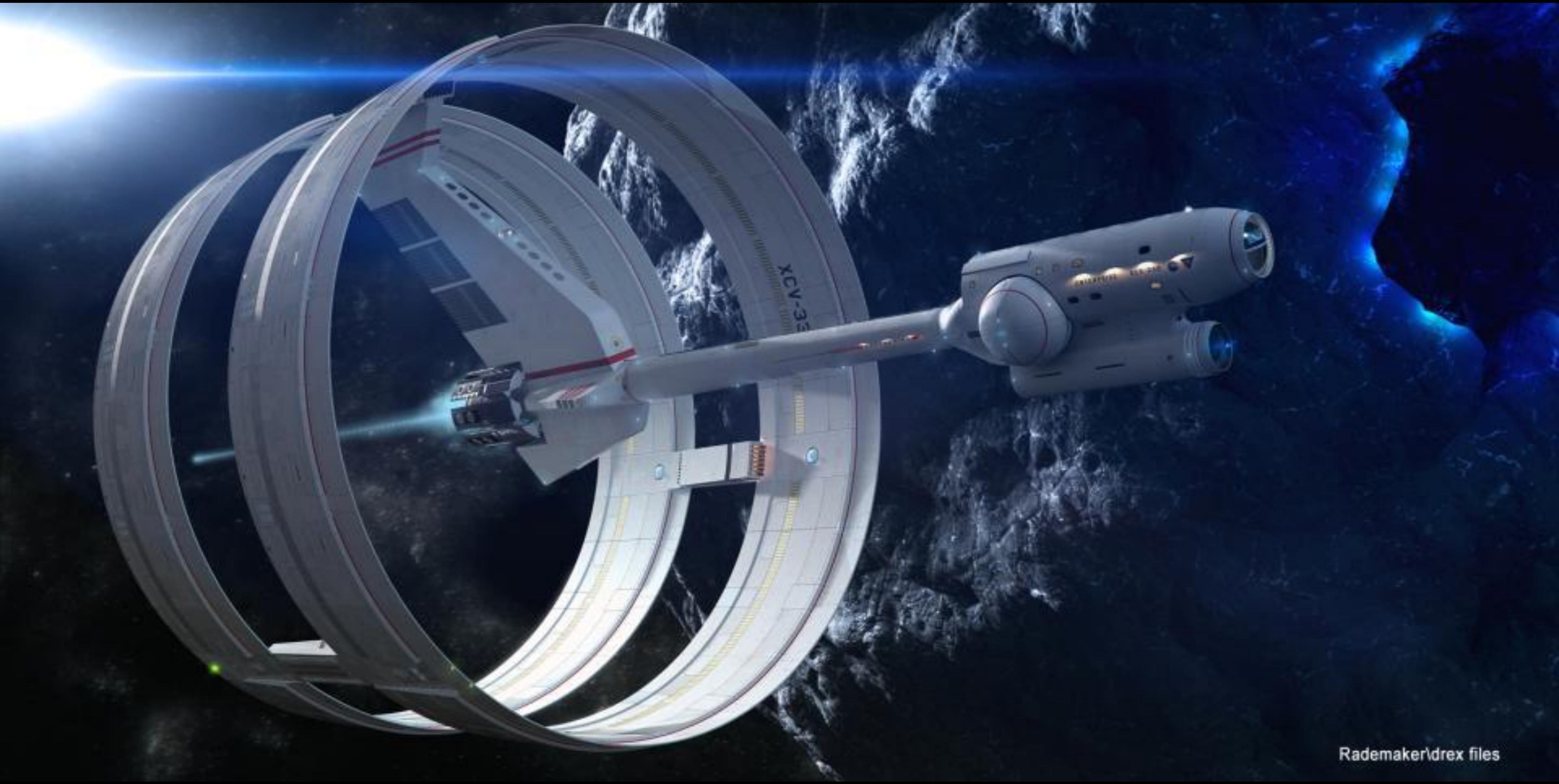

Matthew Jeffries is the artist that created the familiar Star Trek enterprise look

Updated concept based on Dr. White's theoretical findings, rendered by Mark Rademaker with artwork and inputs from Mike Okuda

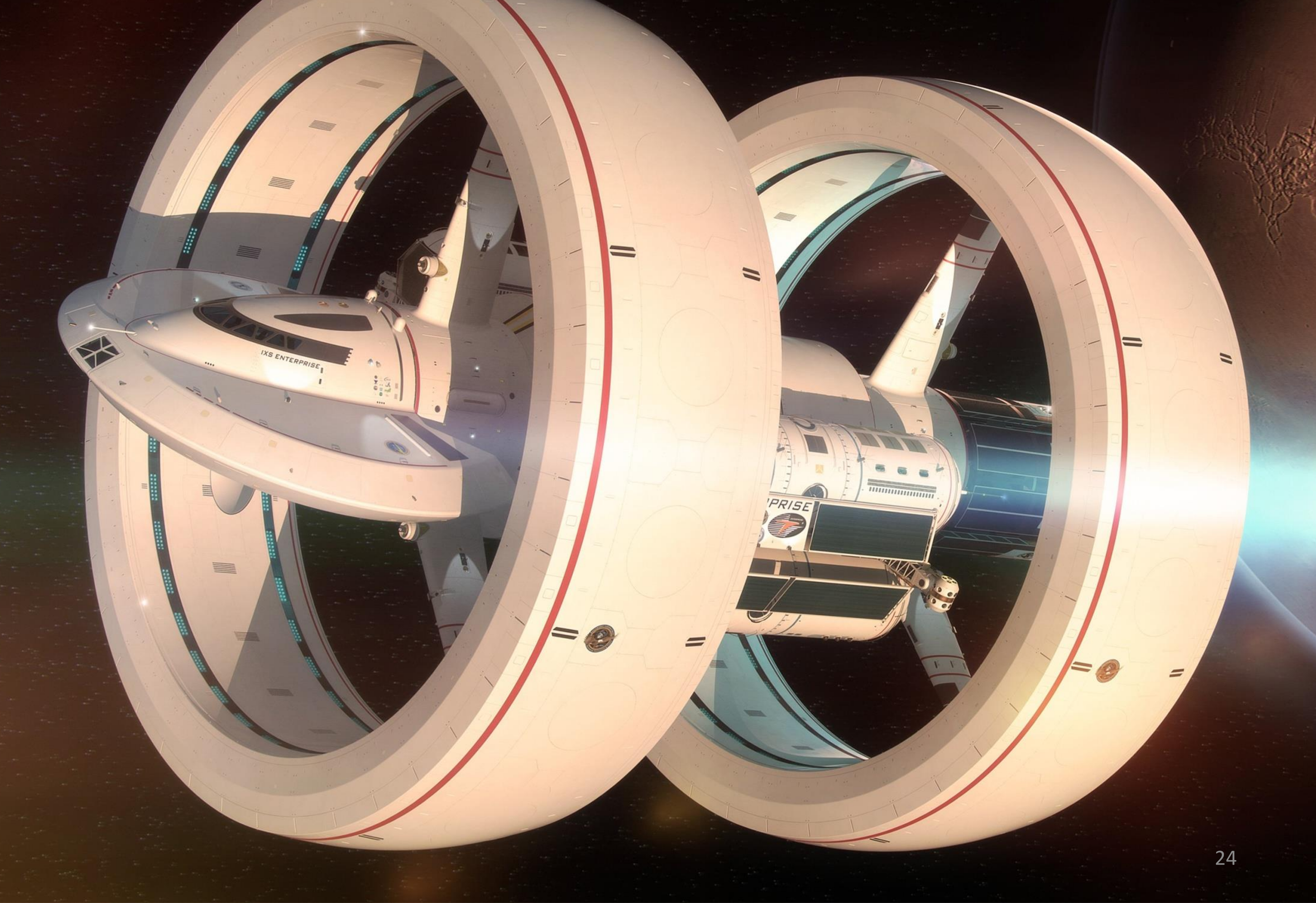

Act II:
Experimental Thrust Measurement of RF Test Articles exploring q-thruster models

Q-Thruster Background

- A Q-thruster is a form of electric propulsion
  - Through the use of electric and magnetic fields, a Q-thruster pushes quantum particles (electrons/positrons) in one direction, while the Q-thruster recoils to conserve momentum
  - This principle is similar to how a submarine uses its propeller to push water in one direction, while the submarine recoils to conserve momentum

- Based on test and theoretical model development, expected thrust to power for initial flight applications is 0.4N/kW (~7x Hall)
  - 0.4 N/kW enables power-constrained HEO SEP missions to close without needing chemical kick stages and very long transit times.
  - 0.4N/kW coupled with persistent power (e.g. NEP) enables rapid transit missions throughout the solar system.

> "If vacuum fluctuations can be harnessed for propulsion by anyone besides science-fiction writers, the purely engineering problems of interstellar flight would be solved." – A.C. Clarke

Torsion Pendulum

Liquid Metal Contacts

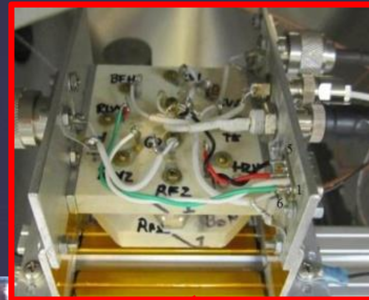

Vacuum ops down to 5x10^-6 Torr

Linear Flexure Bearings

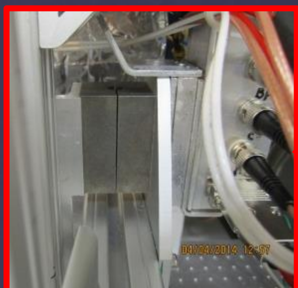

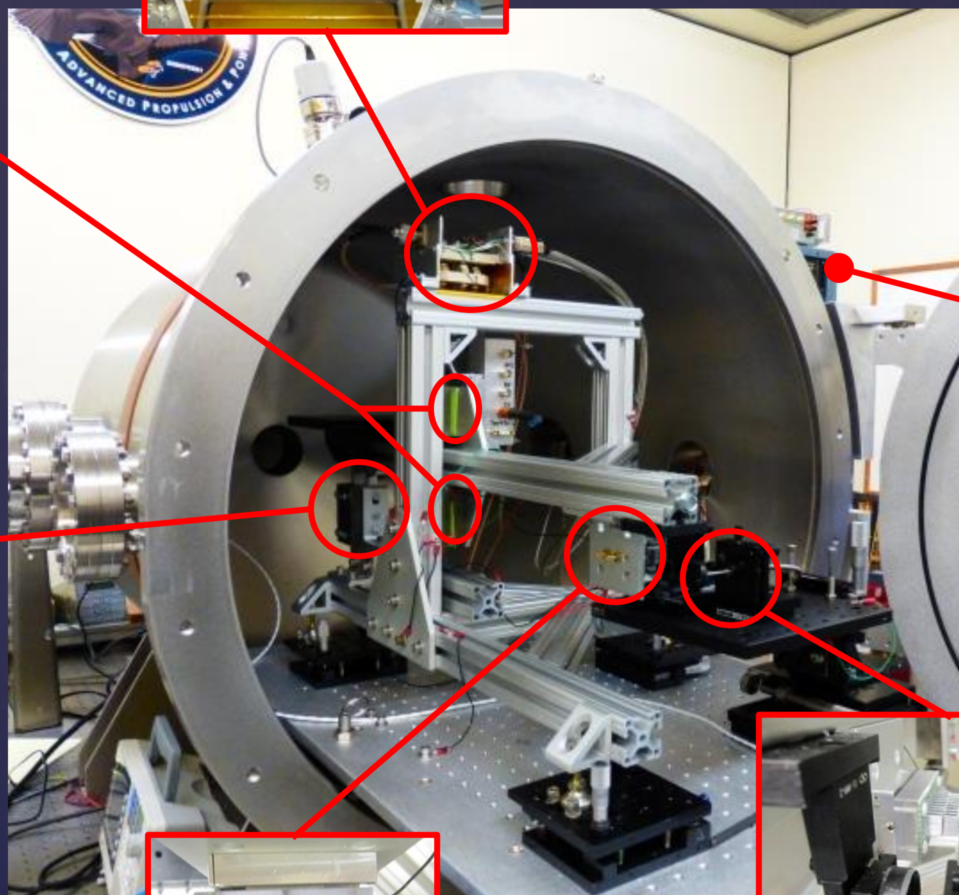

Rackmount DAQ

Magnetic Damper

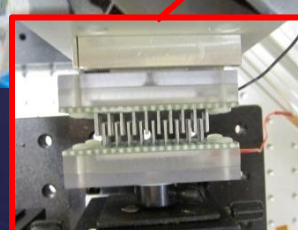

Electrostatic Fins

Linear Displacement Sensor & Adjustment Remote

Cannae RF Test Article

- Test article is a pillbox/beam pipe design fashioned after an RF resonant cavity design used in high energy particle accelerators.
  - Each test article is ~11″ in diameter and 4-5″ between ends of the beam pipes, not counting beam pipe extensions or antenna mounts.
  - Concept is a modified particle accelerator design that incorporates engraved radial slots along the outside edge of the resonant cavity interior, but on only one side of the pillbox (equatorially-asymmetric).
- Cannae theorizes that asymmetric engraved slots would result in a force imbalance (thrust).
- As a result, a second (control) test article was fabricated without the internal slotting dubbed the null test article.

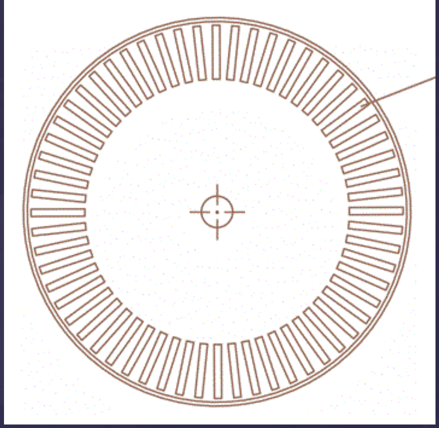

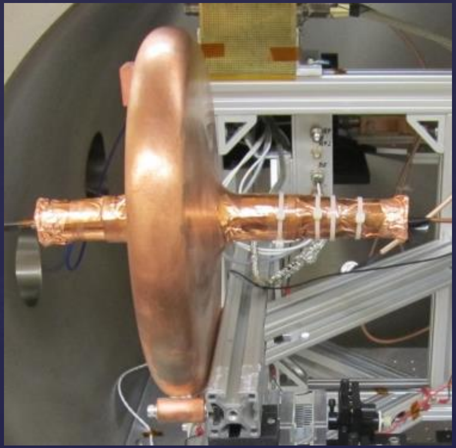

Testing Overview

- RF signal fed into one of test article beam pipes via an approximately 20-gauge copper wire drive antenna.
- On opposite beam pipe, an approximately 20-gauge copper wire serves as a sense antenna for manual tuning during testing.

- The longer beam pipe is the RF drive antenna that in practice ends up being a ¼ wave resonance system in its own right and has a dielectric PTFE slug in the throat in both the slotted and null test article.
- It is this characteristic that became an item of further consideration after completion of the test campaign.

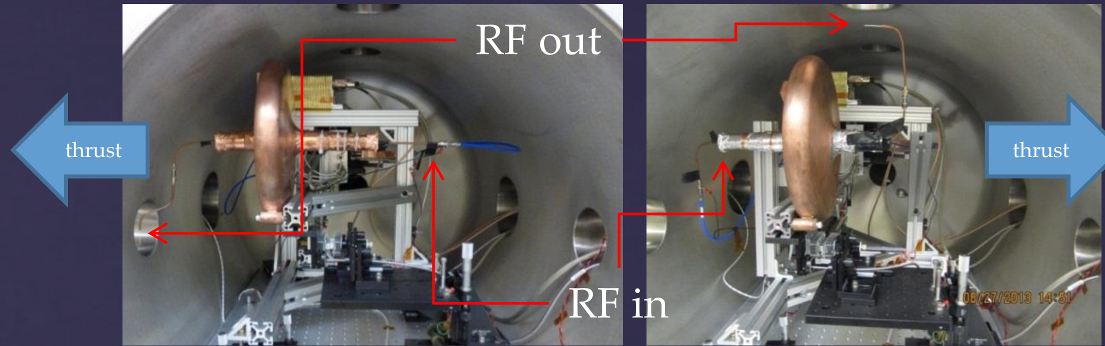

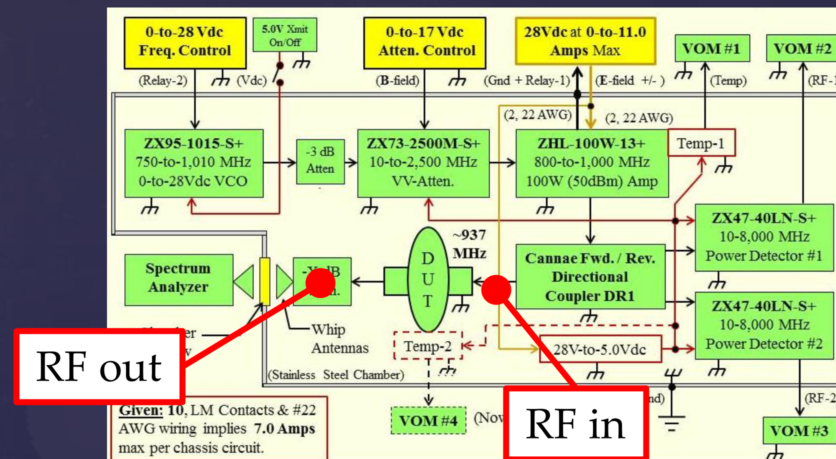

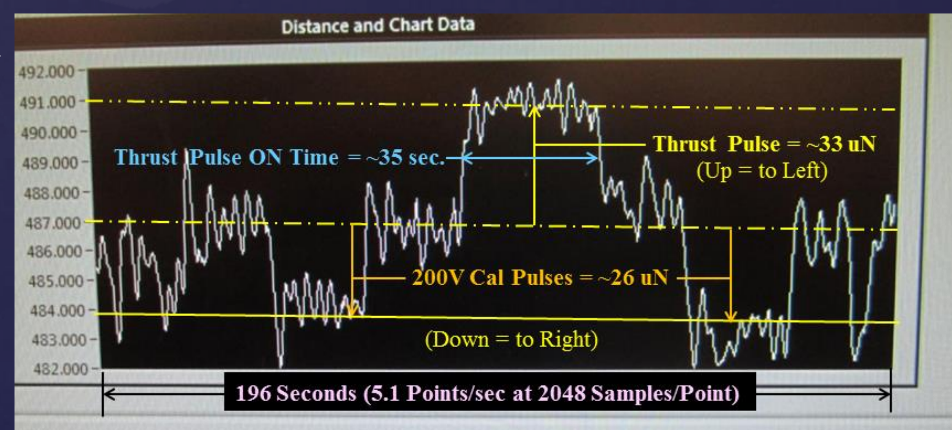

Representative Test Run

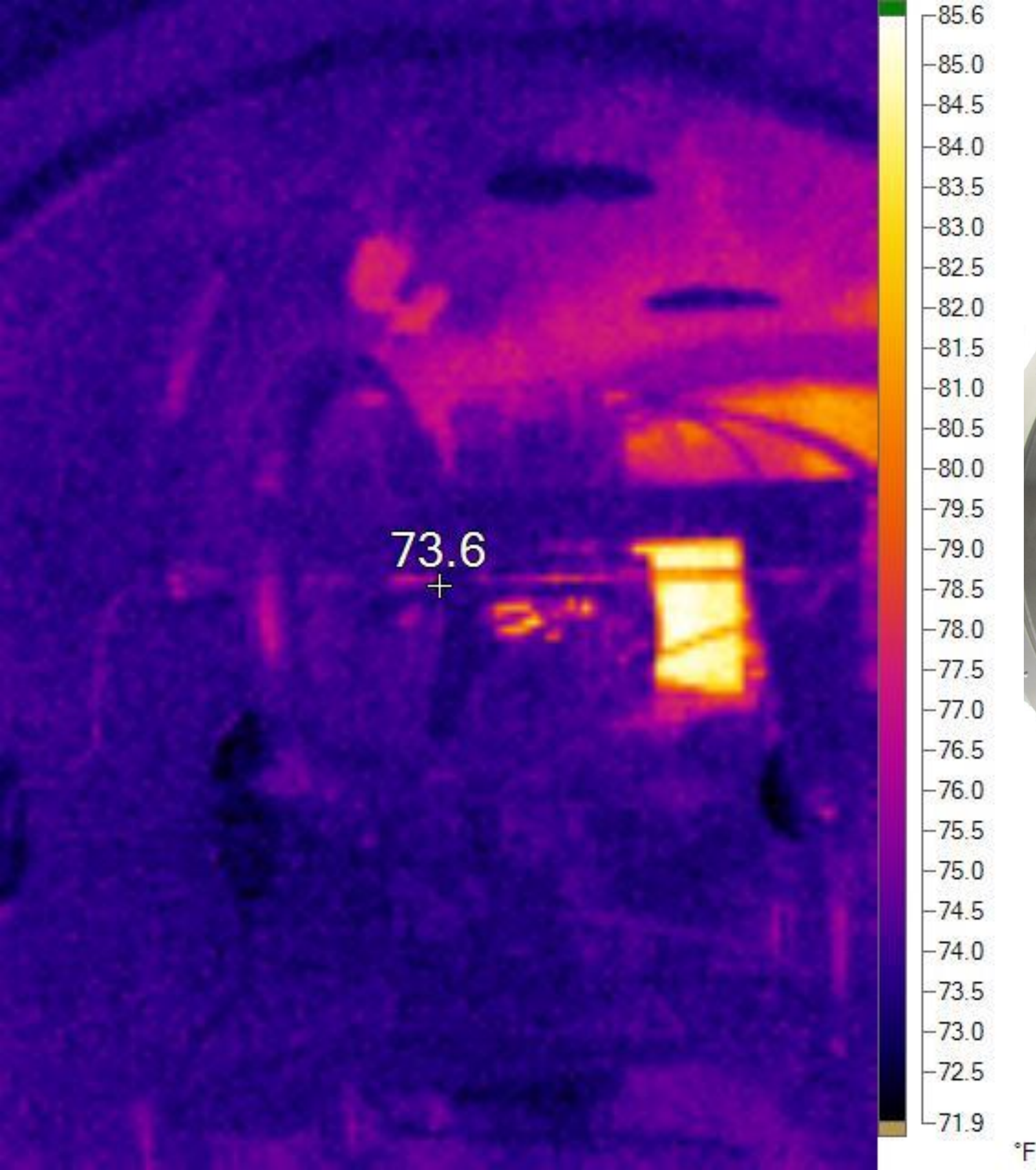

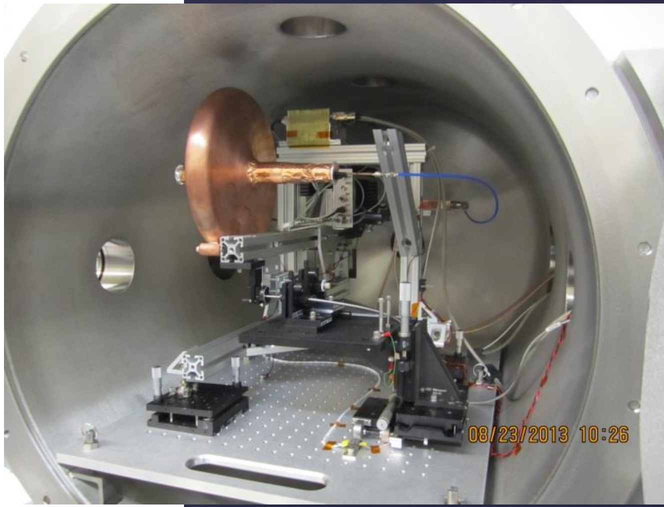

Test article does not get warm during operation (high Q resonance system)
Amplifier kept below 100 F

Cannae Test Results Summary

- The resistive RF Load evaluation indicated no significant systemic cause for torsion pendulum displacement.
- Based upon this observation, both test articles (slotted and unslotted) produced significant thrust in both orientations (forward and reverse).
  - Test schedule constraints prevented multiple data points to be gathered in the reverse orientation, and the single data point for each test article is insufficient to allow comparative conclusions (between slotted and unslotted) to be drawn.
- However, for the forward thrust orientation, the difference in mean thrust between the slotted and unslotted was less than two percent.
- Thrust production did not appear to be dependent on the slotting.

Configuration	Test Article	Thrust Direction	Thrust Range (μN)	Mean Thrust (μN)	Number of Test Runs
1A	Slotted	Forward	31.7 – 45.3	40.0	5
1B	Slotted	Reverse	48.5	48.5	1
2A	Unslotted	Forward	35.3 – 50.1	40.7	4
2B	Unslotted	Reverse	22.5	22.5	1
RF Load	50Ω Load	N/A	0.00	0.00	2

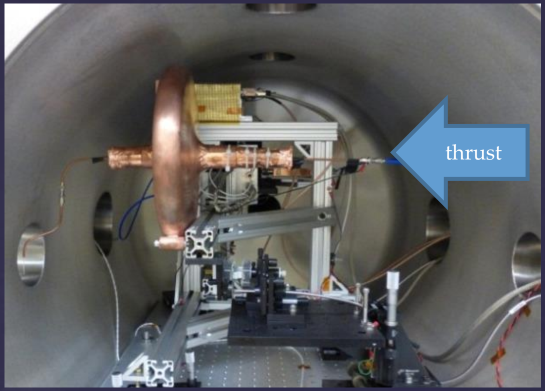

Configuration 1A

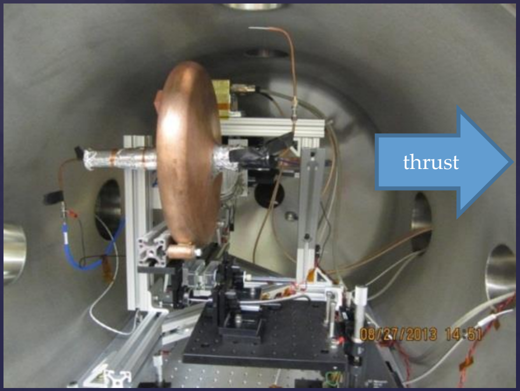

Configuration 2B

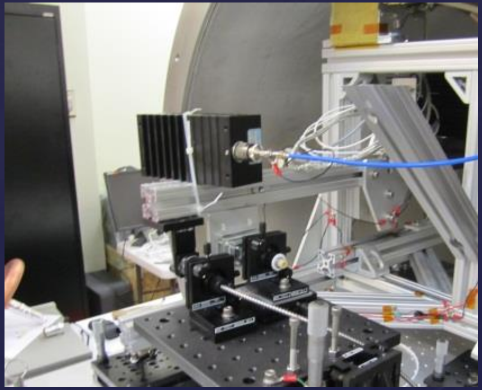
RF Dummy Load

COMSOL Analysis of Cannae Test Articles

- Computer modeling of the electric field within the pillbox and beam pipe illustrates weakness of electric field in vicinity of cavity slots and relative strength of the electric field within the beam pipe, especially in the drive antenna coaxial cable and the region around the cable within the PFTE dielectric slug as seen in the following figure.

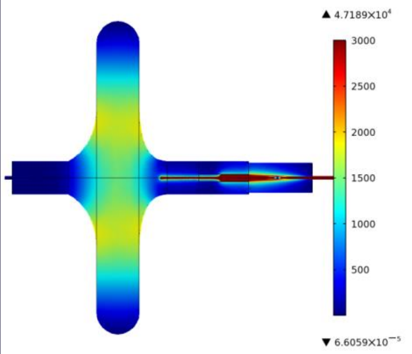

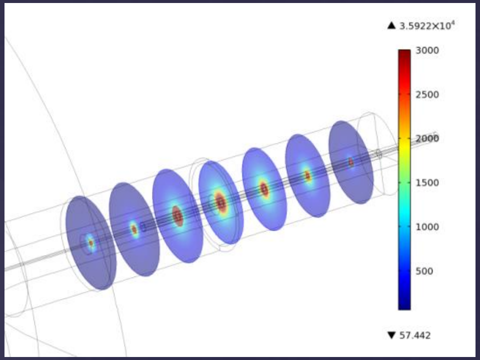

- Consideration of the dynamic fields in the ¼ wave resonance tube shows that there is always a net Poynting vector meaning that the RF launcher tube assembly with dielectric cylinder common to both the slotted and smooth test articles was potentially a Q-thruster where the pillbox is simply a matching network.

- The predicted thrust using the Q-thruster analytic model is 34 micronewtons with input power of 25 Watts and Quality factor of 8000.

Tapered RF Q-thruster

- Just like there are many ways to build a race car motor, there are many ways to build a thruster, or in this case, a Q-thruster.
- The figures depict one of the early COMSOL models representing an early possible construction of a tapered RF unit alongside the actual construction that was finally implemented as informed by the COMSOL findings.
- The tapered RF geometry was explored as it pertains to some recent findings published by the Northwest Polytechnical University.

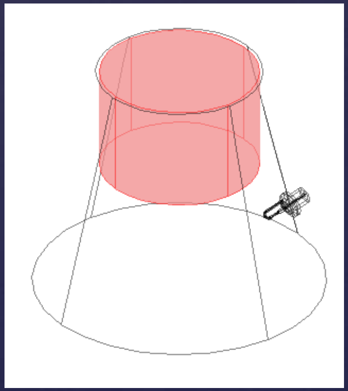

4″ dielectric resonator

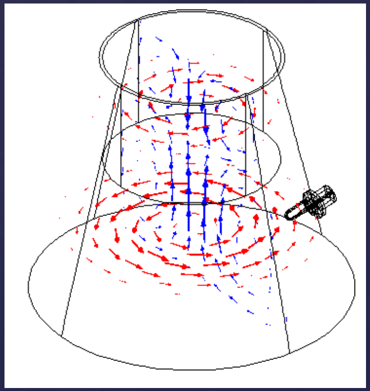

TE012 mode

Test article

Copper Frustum TM212, 1,937.115 MHz Test Setup

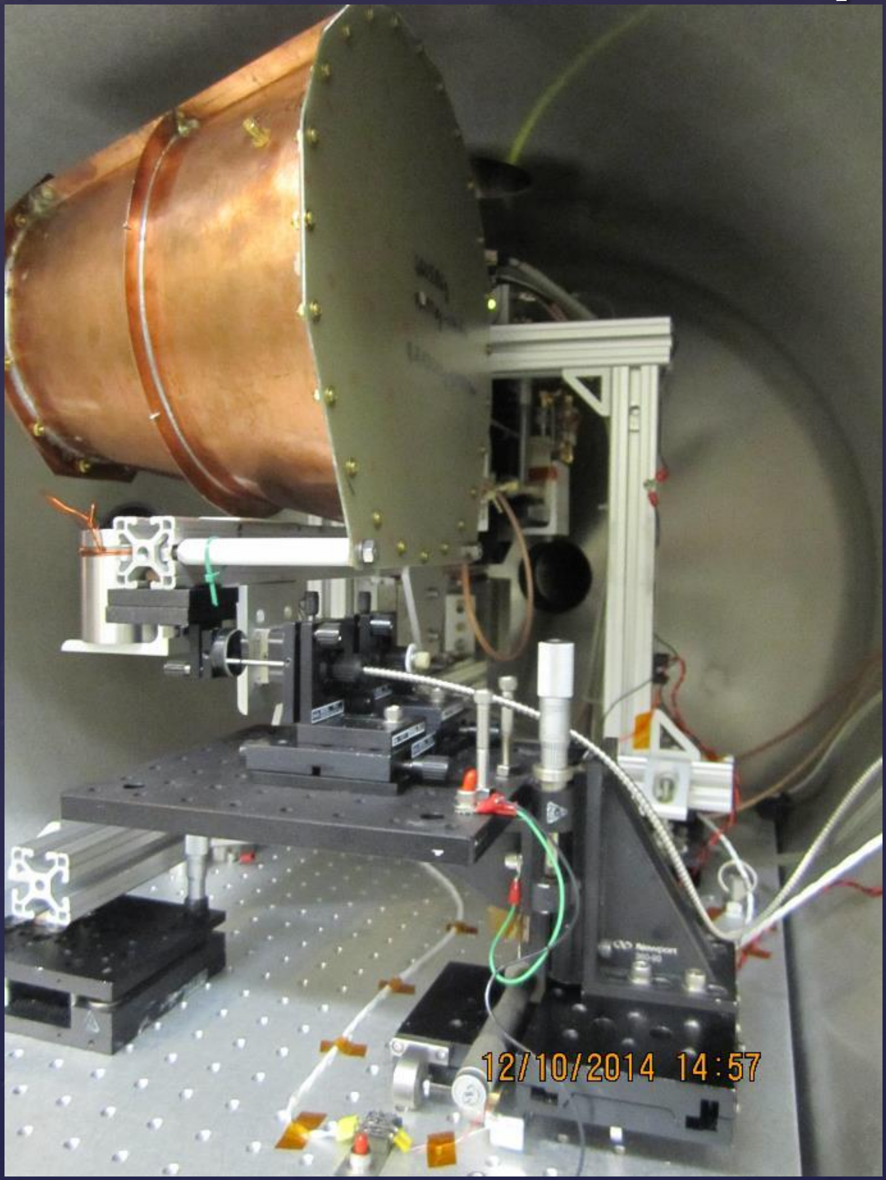

Pendulum Systemic Noise Setup-4

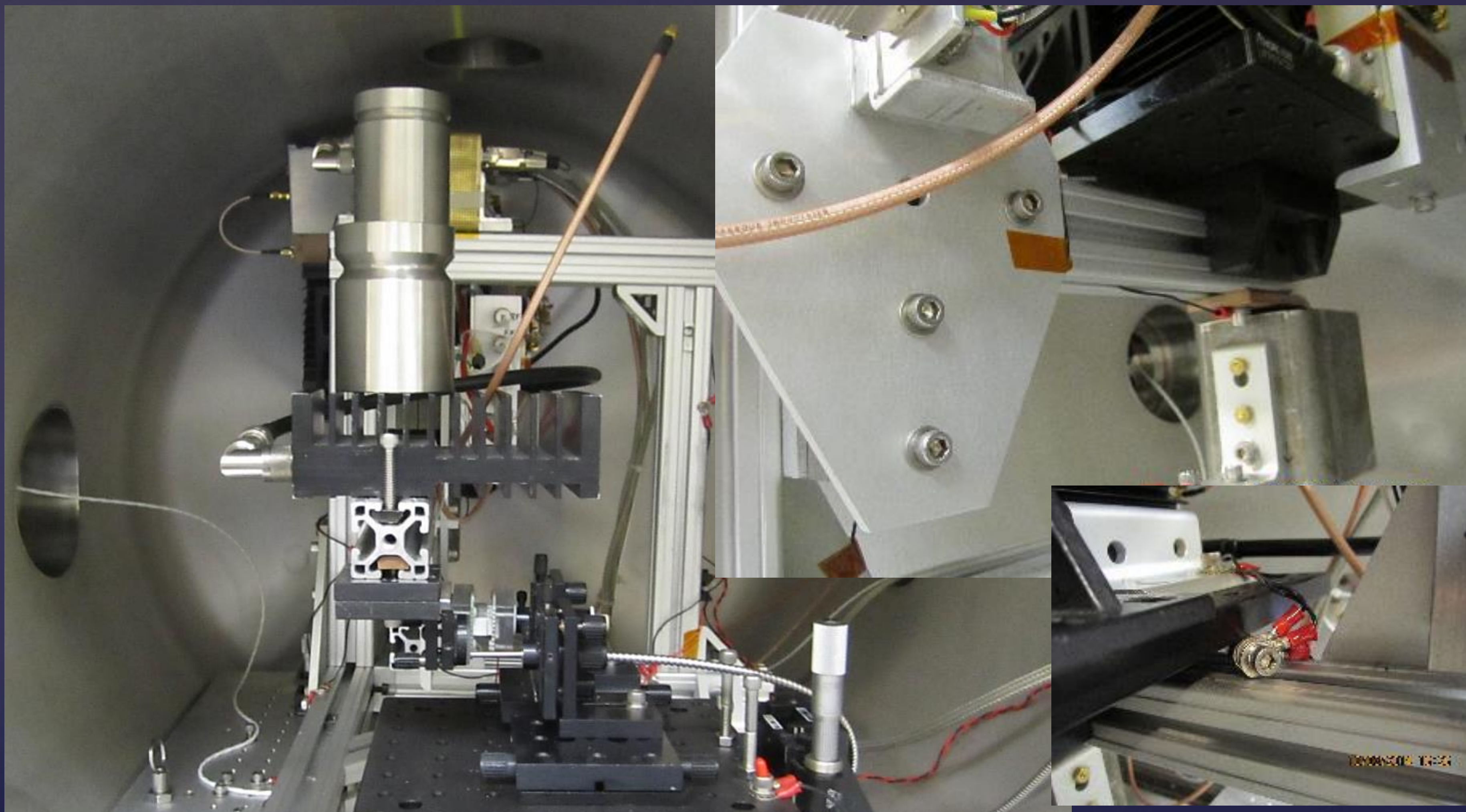

Systemic Forces on the Pendulum-4

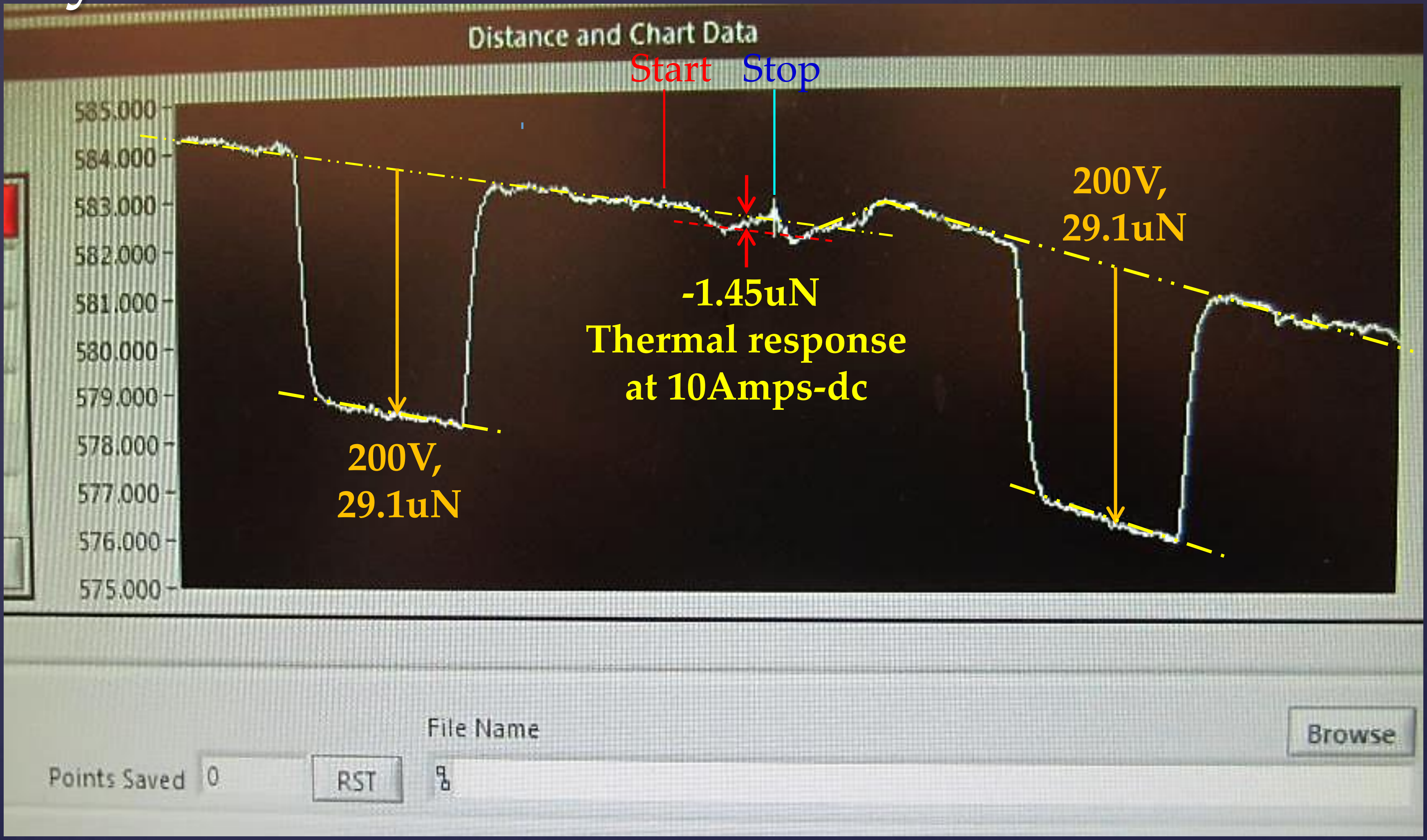

COMSOL RF Analysis

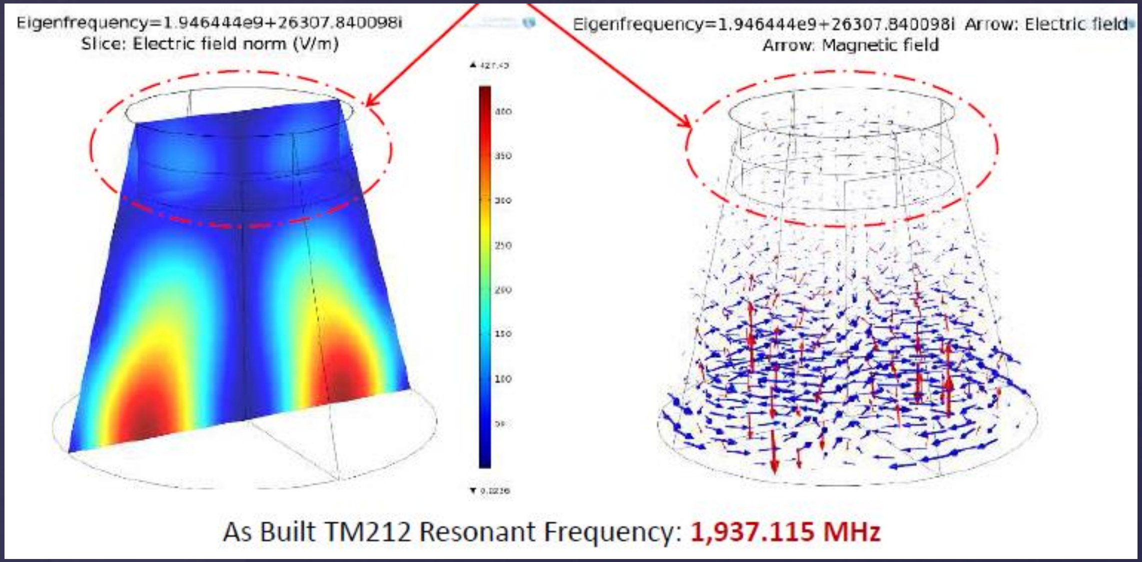

COMSOL Thermal vs Observation

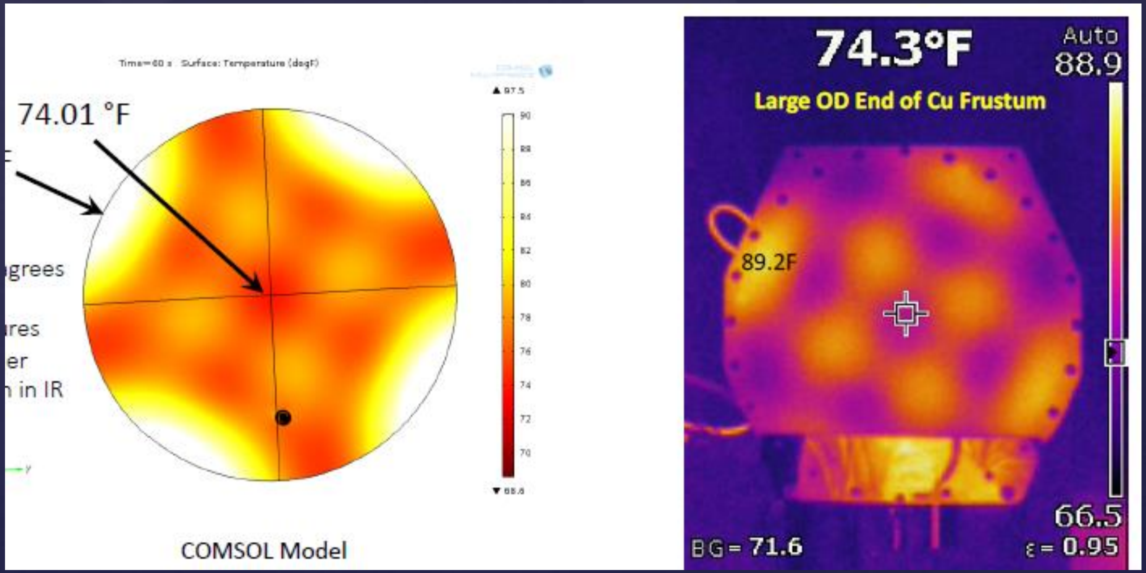

TM212, 1,937.115MHz, ~30W, Q_L=6,726, ~5x10^{-6} Torr

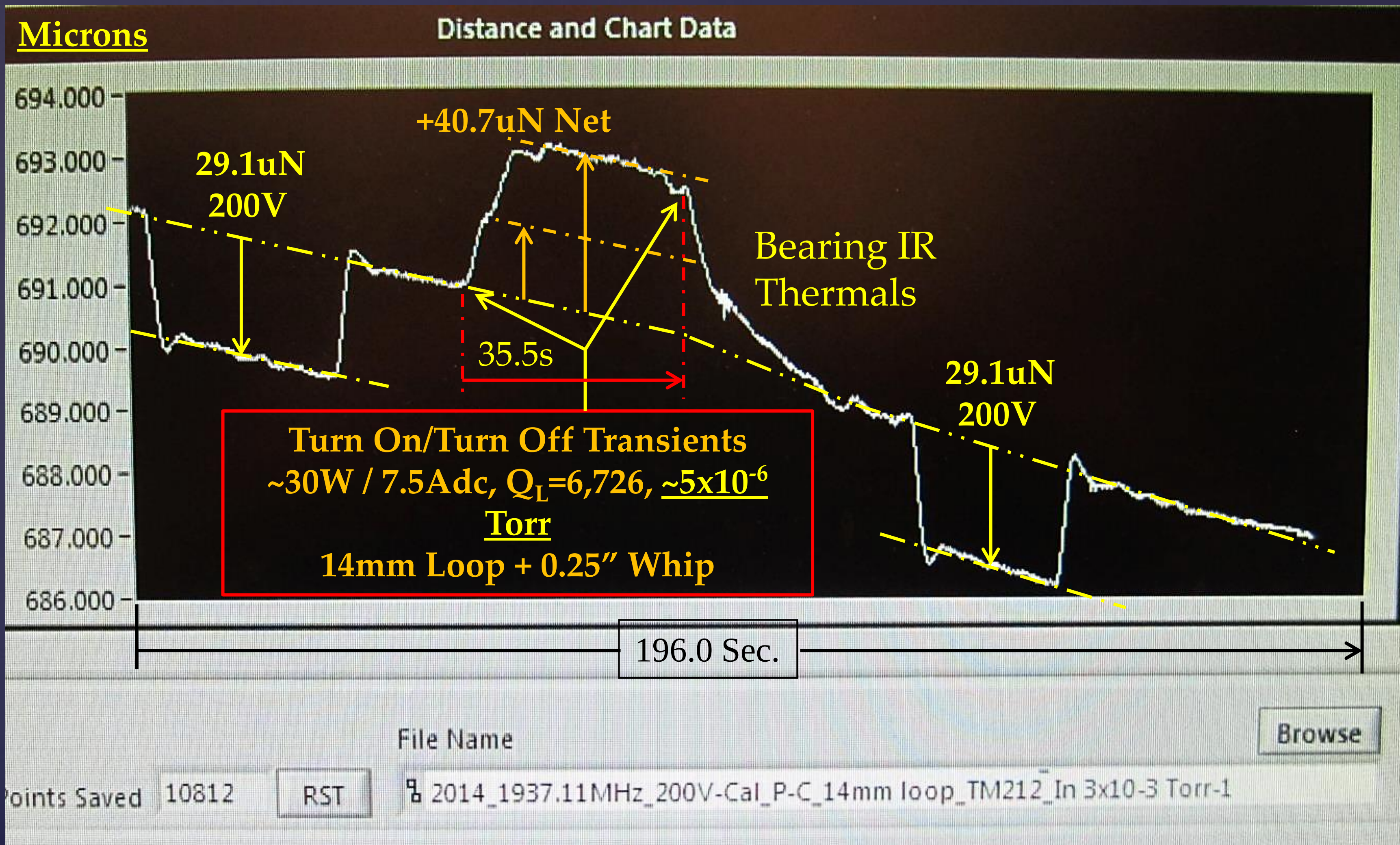

TM212, 1,937.115MHz, ~35W, Q_L=6,726, ~5x10^{-6} Torr

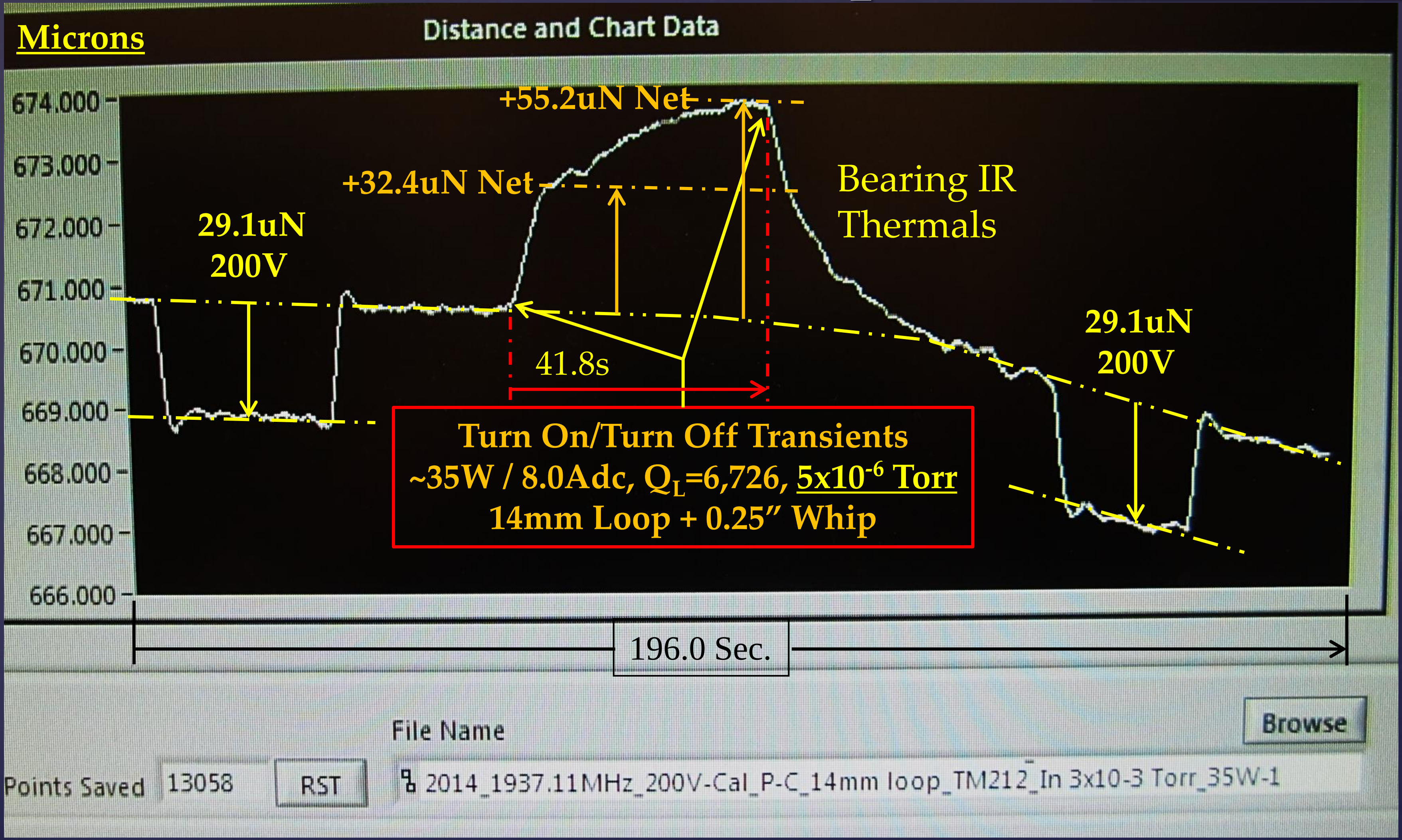

TM212, 1,937.115MHz, ~40W, Q_L=6,726, ~5x10^{-6} Torr

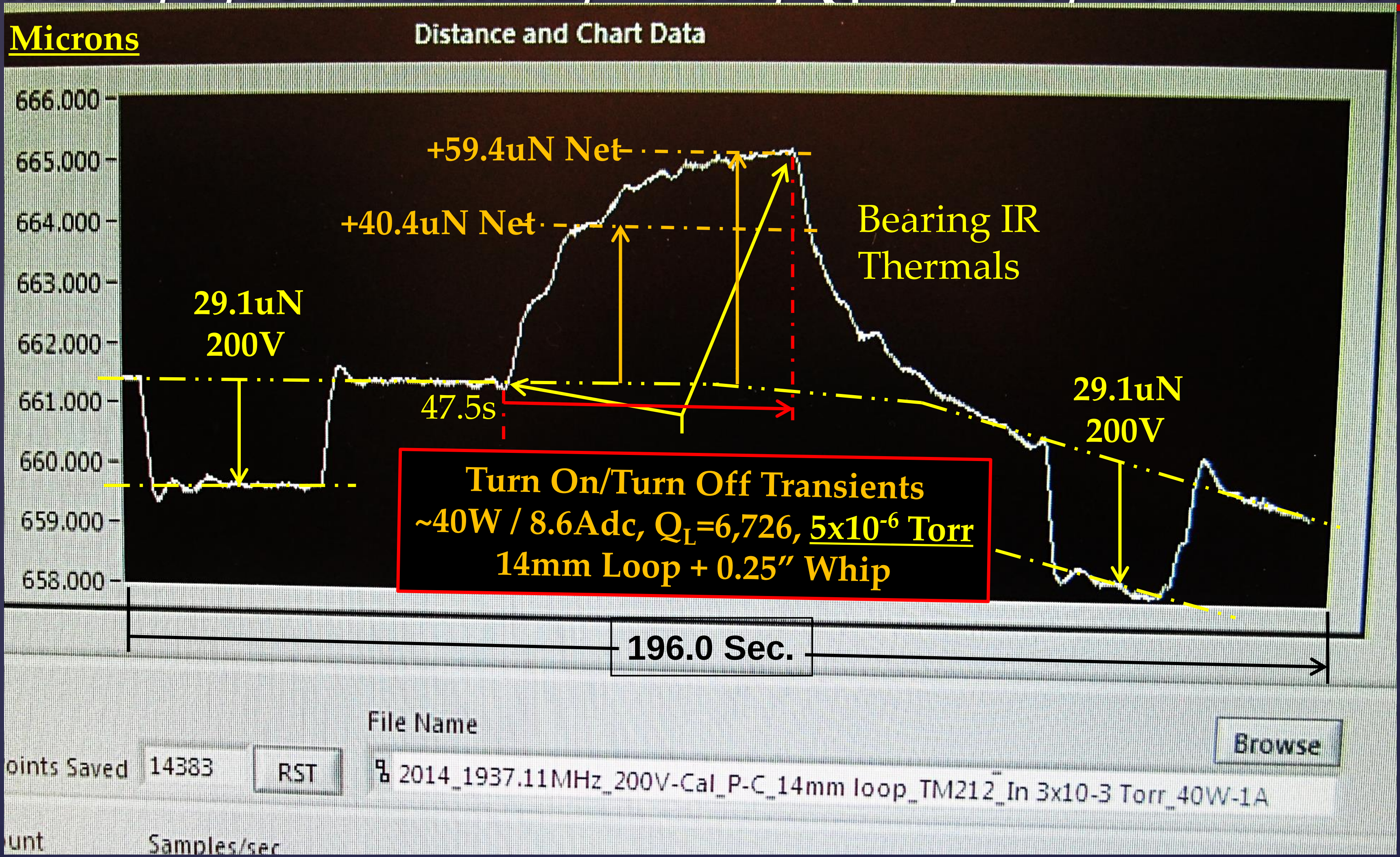

TM212, 1,937.115MHz, ~45W, Q_L=6,726, ~5x10^{-6} Torr

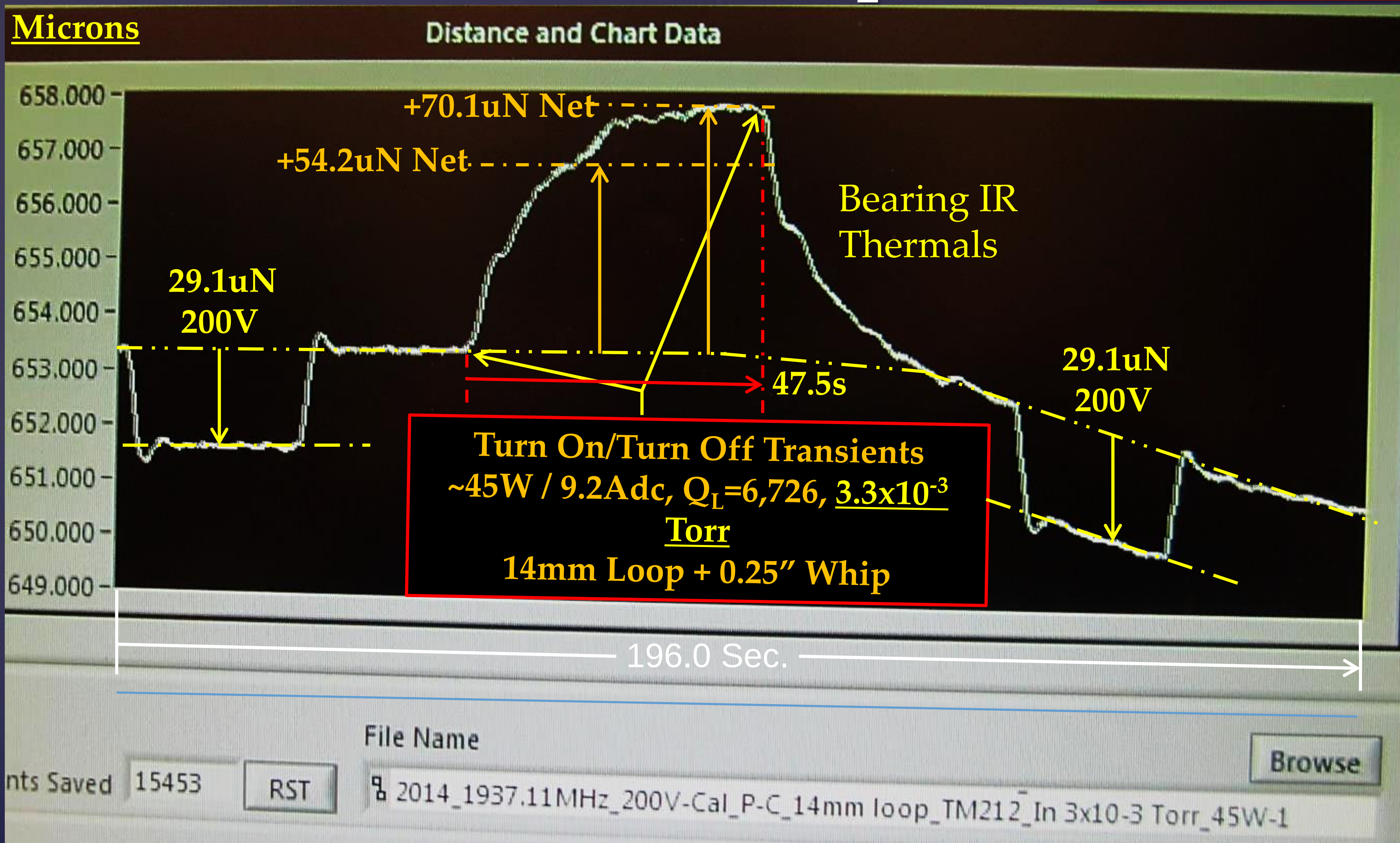

TM212, 1,937.115MHz, ~50W, Q_L=6,726, ~5x10^{-6} Torr

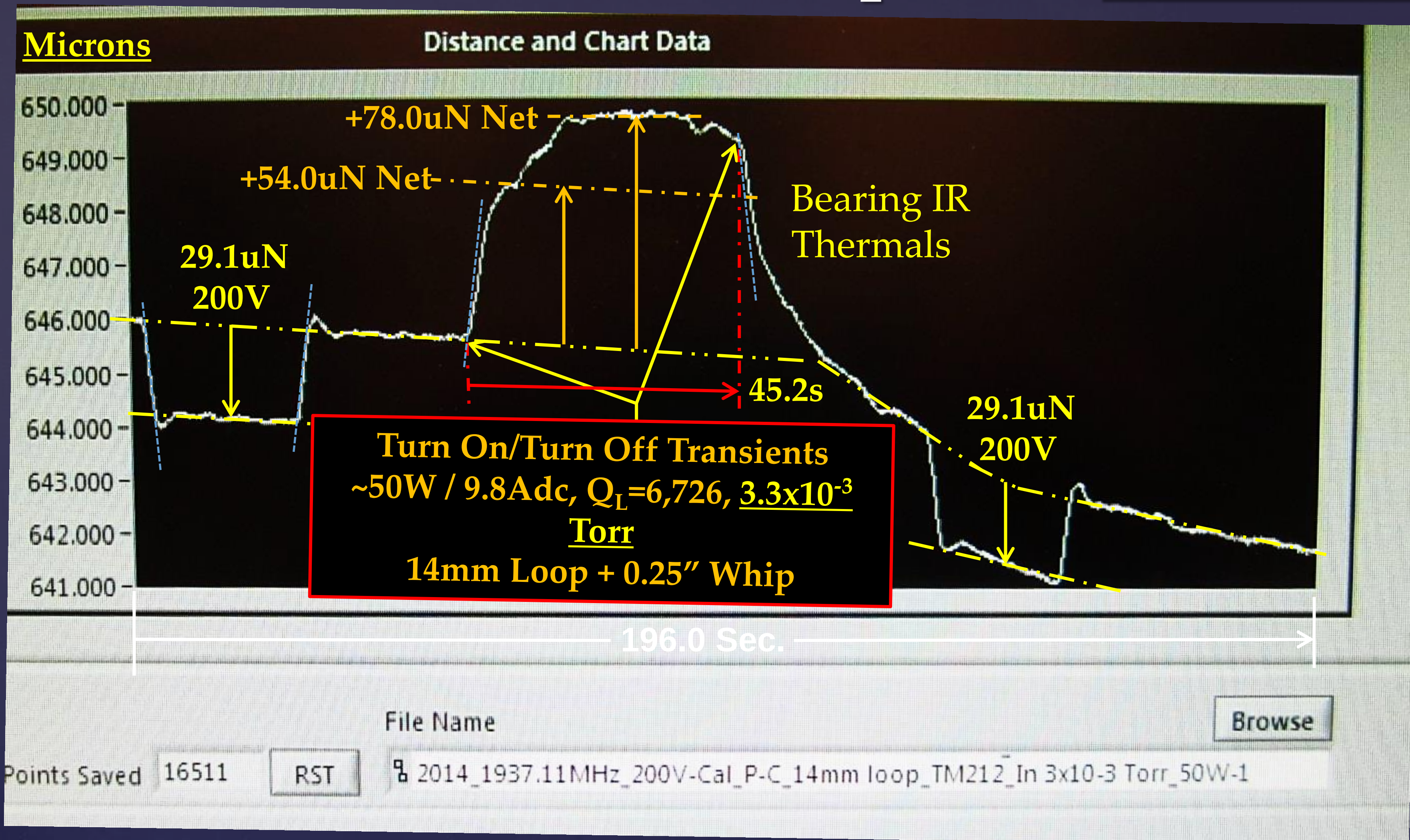

Forward Thrust Campaign

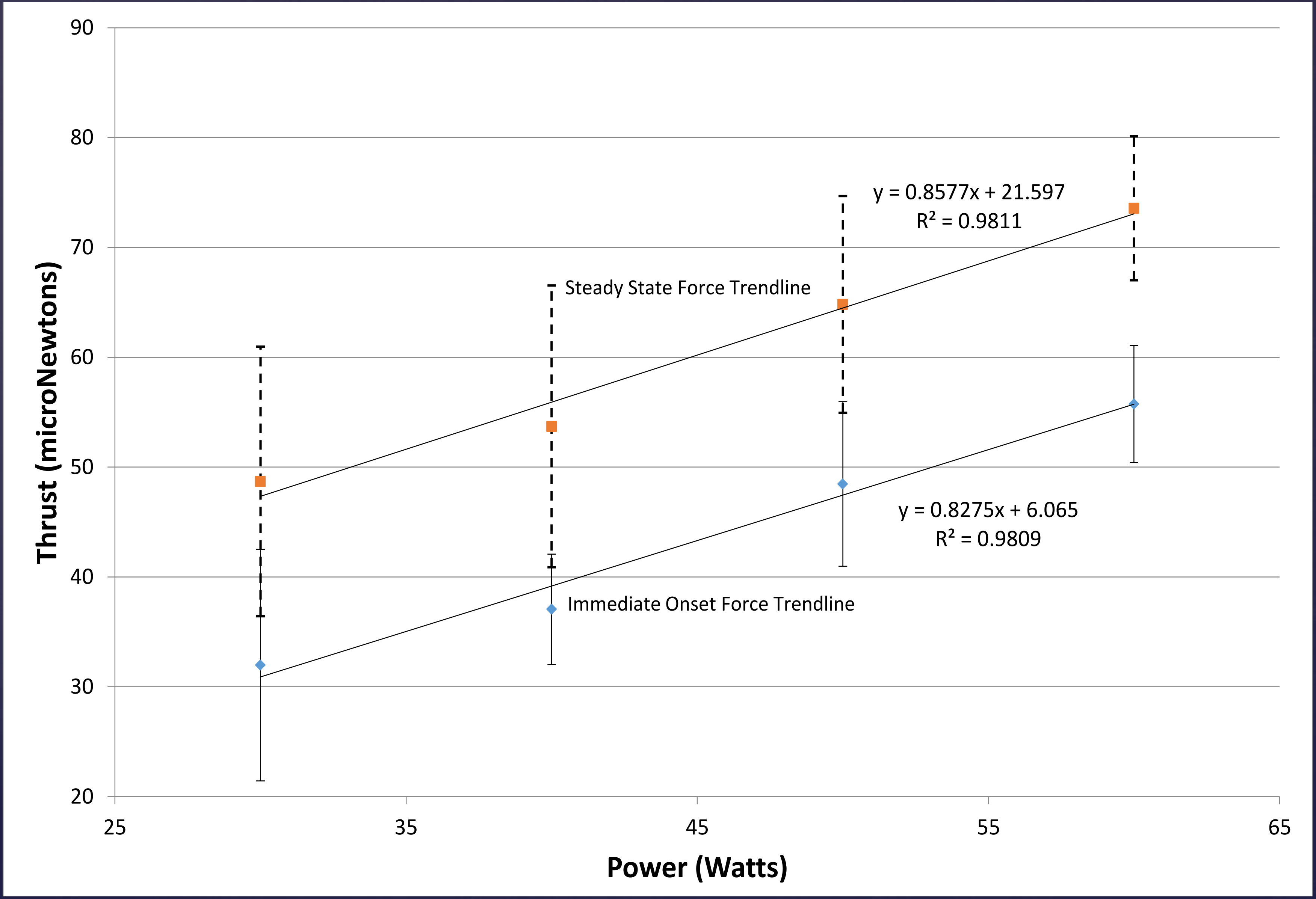

FORWARD WORK

- JSC: Complete the vacuum test campaign

- Perform an IV&V test campaign at the Glenn Research Center using their low thrust torsion pendulum followed by a possible repeat campaign at the Jet Propulsion Laboratory using their low thrust torsion pendulum.

- The Johns Hopkins University Applied Physics Laboratory has also expressed an interest in performing a Cavendish Balance style test with the IV&V shipset.

GRC Torsion Pendulum

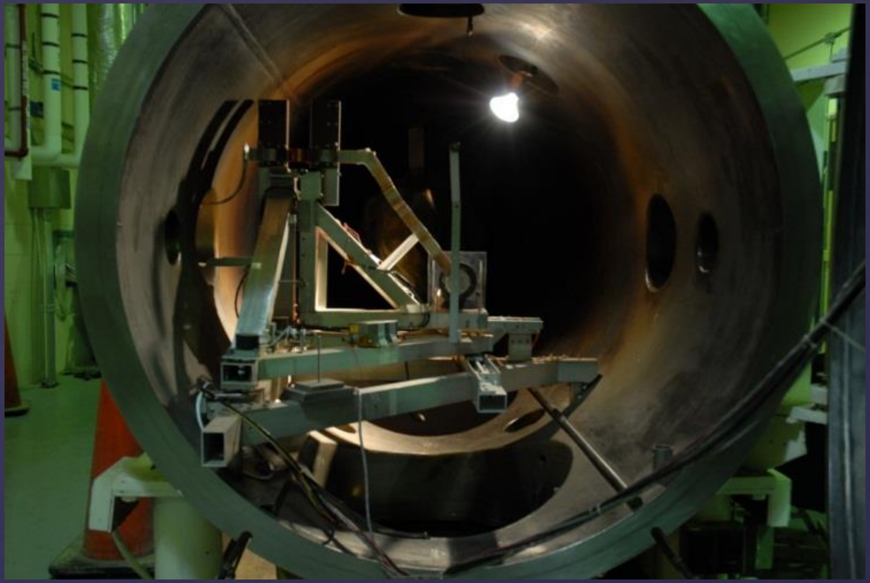

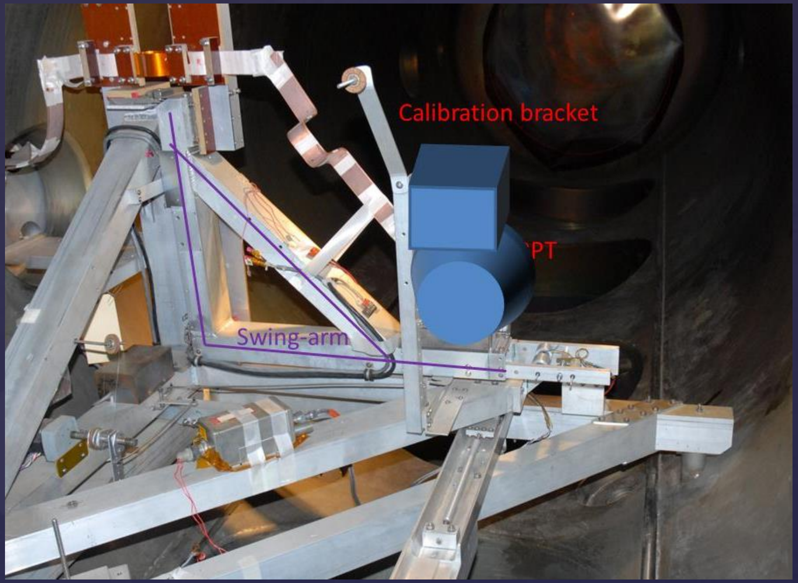

Act III:
Value Proposition

- Dawn propulsion & power system
  - Three NSTAR xenon ion thrusters
  - 0.04 N/kWe thrust-to-power ratio
  - ~90 mN/thruster
  - 2.3 kWe solar power at 1 AU
  - 425 kg of xenon propellant

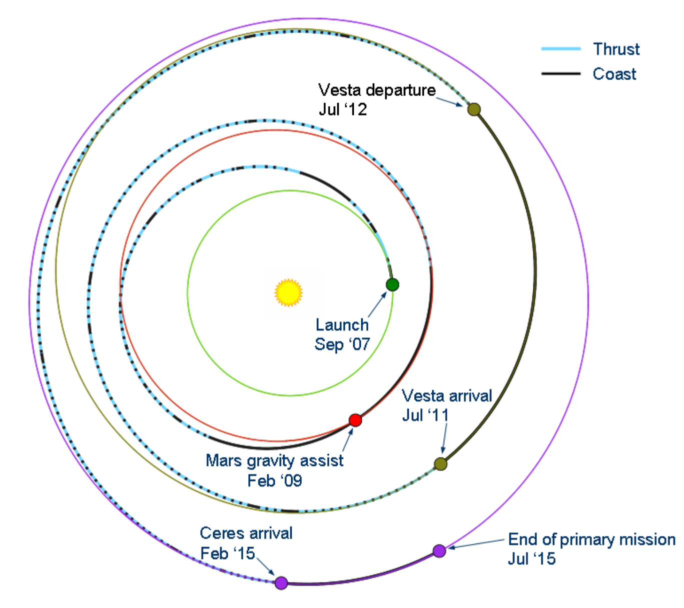

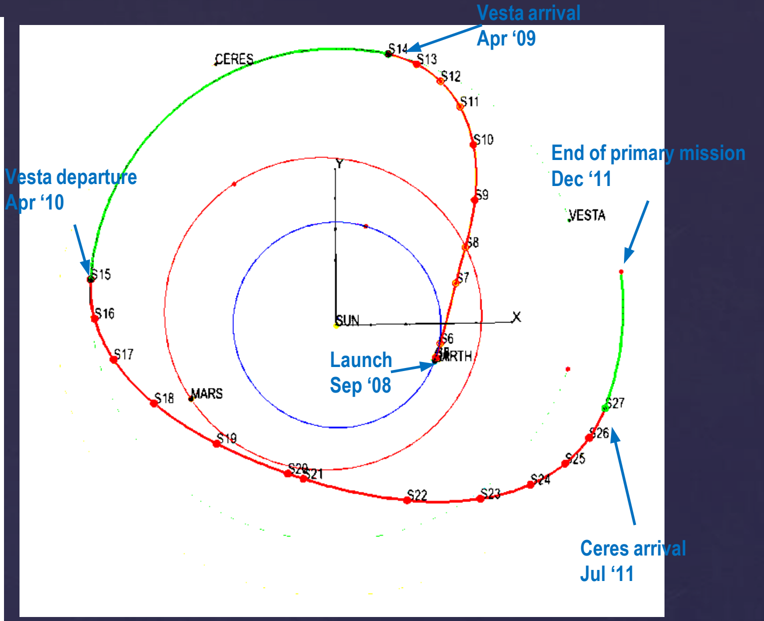

Dawn with 2.3kWe Ion Thrusters

Dawn with 2.3kWe Q-thrusters

Activity	Dates	Segment (months)	Elapsed (months)	Dates	Segment (months)	Elapsed (months)
Earth to Vesta	Sep 2007 – Jul 2011	46	46	Sep 2008 – Apr 2009	7 (15% of ion)	7
Vesta orbit	Jul 2011 – Jul 2012	12 (fixed)	58	Apr 2009 – Apr 2010	12 (fixed)	19
Vesta to Ceres	Jul 2012 – Feb 2015	31	89	Apr 2010 – Jul 2011	15 (48% of ion)	34
Ceres orbit	Feb-Jul 2015	5 (fixed)	94 (7.8 yrs)	Jul-Dec 2011	5 (fixed)	39 (3.3 yrs) (41%)

300 kW SEP Mars

- 70t stack departs from DRO
- 300kW SEP
- 0.4N/kW Q-thrusters
- 50-day stay in Deimos orbit around Mars
- Total mission duration of 788 days and 2AU maximum distance from the sun.

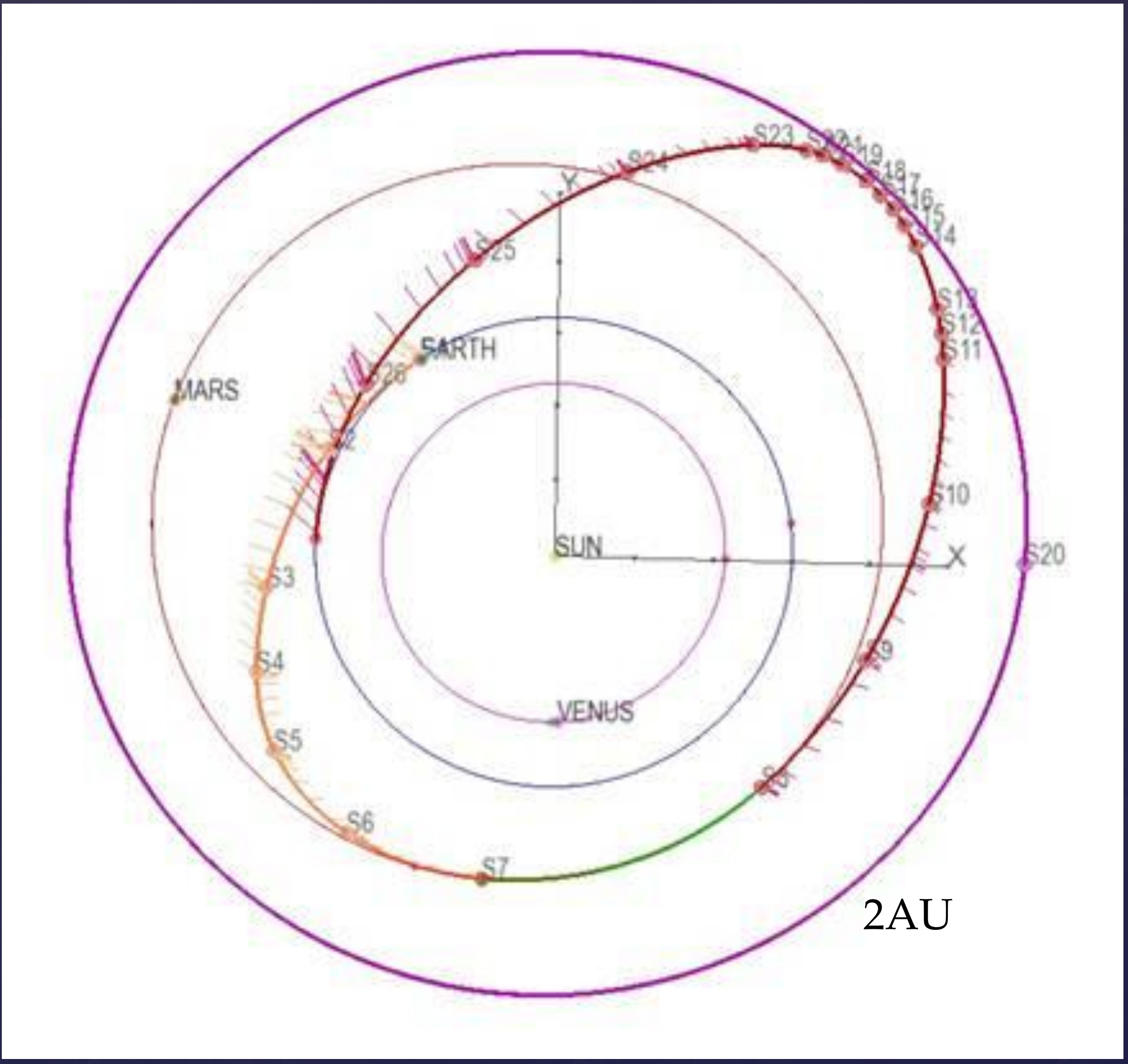

2MW NEP Mars

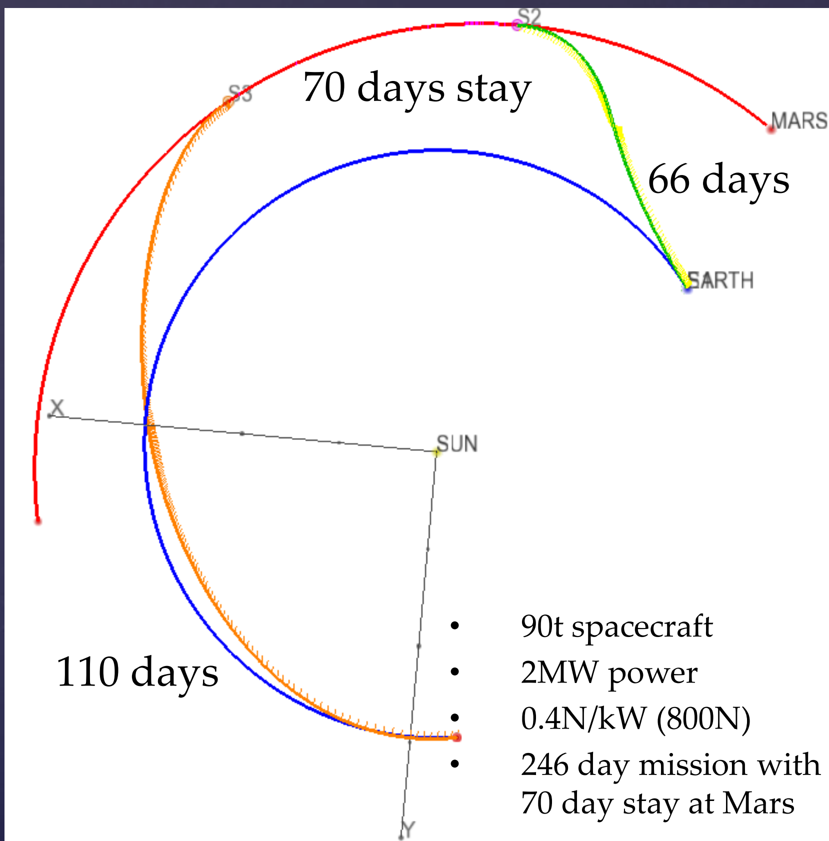

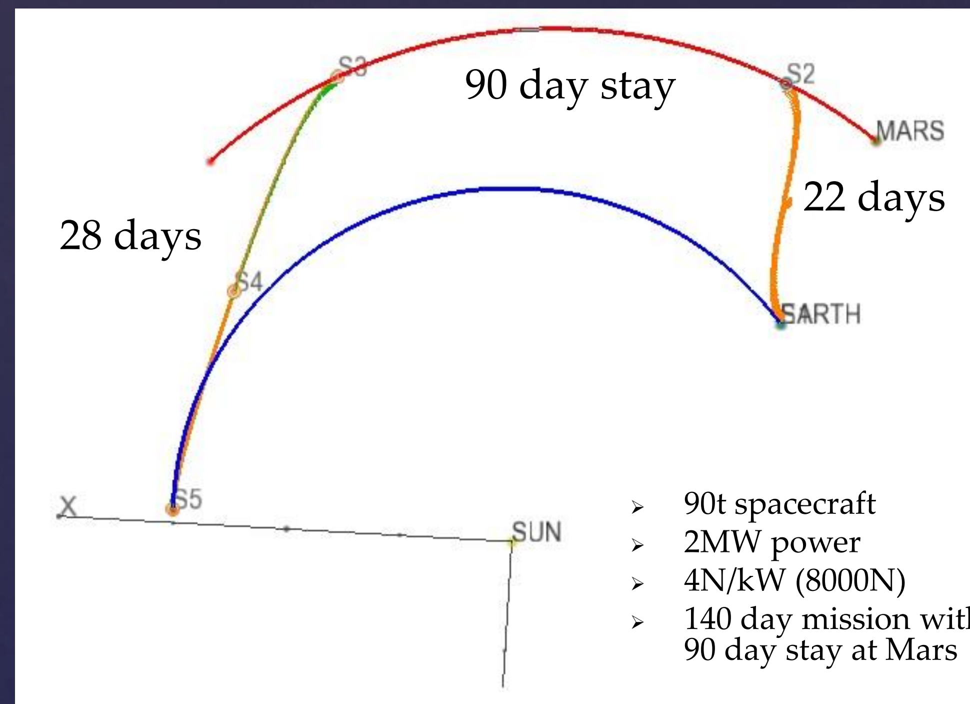

<u>90t spacecraft:</u>

- 50t cargo
- 20t 2MW nuclear reactor (10 kg/kW)
- 20t Q-thruster bank (10kg/kW)

Crewed Titan/Enceladus Mission

- Same vehicle characteristics as Jupiter mission assumed
- Trip time to/from Saturn ~9 months each way, 6 month stay in Europa vicinity, 6 month stay in Enceladus vicinity. 32-month total mission.
- Shorter than "current" conjunction-class *Mars* missions

Assuming:
T_s=0.4 N/kWe
P=2000 kWe
α_{power}=10 kg/kWe
α_{prop}=10 kg/kWe
m_{pl} = 50t

T/m =0.91 m-g's

Vehicle mass = 90 t

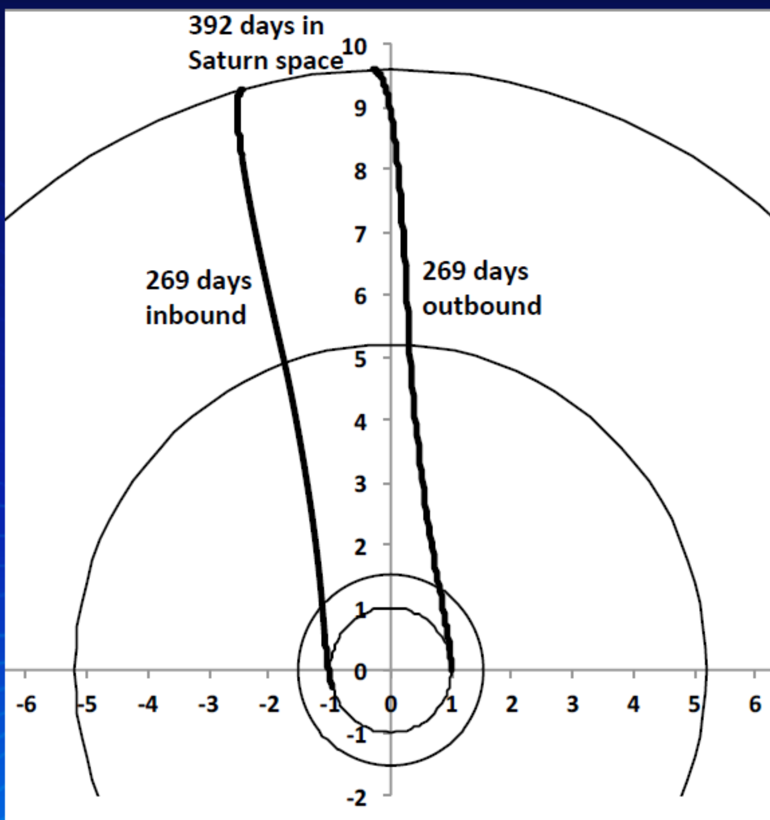

Segment	Flight Time
LEO to C_3=0	10 days
Earth-Saturn	269 days
C_3=0 to Titan	7 days
Loiter at Titan	180 days
Titan to Enceladus	9 days
Loiter at Enceladus	180 days
Enceladus to C_3=0	16 days
Saturn-Earth	269 days
C_3=0 to LEO	10 days
Total	950 days

By comparison: Even utilizing NTR-levels of performance, these missions would be infeasible

Act IV:
Dynamics of the Vacuum and Casimir Analogs to the Hydrogen Atom

Principles of Q-thruster Operation

- Principle 1: Local mass concentrations, say in the form of a conventional capacitor with a ceramic dielectric, affect vacuum fluctuation density according to equation 1

$$\rho_{v\_local} = \rho_v \sqrt{\frac{\rho_{m\_local}}{\rho_v}} = \sqrt{\rho_{m\_local}\rho_v} \qquad (1)$$

- Principle 2: Just as relativistic acceleration (Unruh radiation) can change the apparent relative density of the vacuum, so too can higher order derivatives according to equation 2.

$$\delta\rho = \frac{1}{4\pi G}\left(-\frac{1}{a^2}\left(\frac{da}{dt}\right)^2 + \frac{1}{a}\frac{d^2a}{dt^2}\right)$$

$$\vec{a} = -\nabla\phi$$

$$\delta\rho = \frac{1}{4\pi G}\left(\frac{1}{\phi^2}\left(\frac{d\phi}{dt}\right)^2 - \frac{1}{\phi}\frac{d^2\phi}{dt^2}\right) \qquad (2)$$

- Principle 3: The tools of MagnetoHydroDynamics (MHD) can be used to model this modified vacuum fluctuation density analogous to how conventional forms of electric propulsion model propellant behavior.

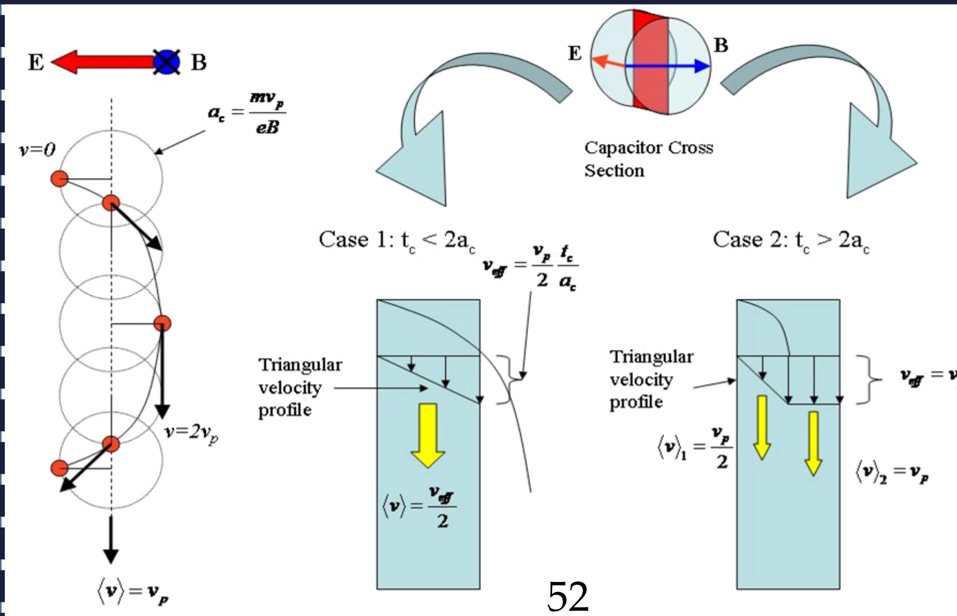

TABLE I: This table shows the derived "density" of a given energy state n, with $Z = 1$

n [a]	$radius(m)$	$E(eV)$	$E(J)$	$\rho\left(kg/m^3\right)$
1	5.29×10^{-11}	13.60	2.176×10^{-18}	3.905×10^{-5}
2	2.11×10^{-10}	3.40	5.440×10^{-19}	1.525×10^{-7}
3	4.76×10^{-10}	1.51	2.418×10^{-19}	5.952×10^{-9}
4	8.46×10^{-10}	0.85	1.360×10^{-19}	5.959×10^{-10}
5	1.32×10^{-9}	0.54	8.704×10^{-20}	9.997×10^{-11}
6	1.90×10^{-9}	0.38	6.044×10^{-20}	2.325×10^{-11}
7	2.59×10^{-9}	0.28	4.441×10^{-20}	6.774×10^{-12}

[a] The primary quantum number n is only varied from 1 to 7 here.

$$r_n = \frac{4\pi\epsilon_0 n^2\hbar^2}{e^2 m_e} = n^2\ 5.29{\times}10^{-11} meters,\ n = 1, 2, 3, ...$$

$$E_n = -\left[\frac{m}{2\hbar}\left(\frac{e^2}{4\pi\epsilon_0}\right)^2\right]\frac{1}{n^2} = -\frac{1}{n^2}13.6eV,\ n = 1, 2, 3, ...$$

$$r_{Z,n} = \frac{n^2}{Z}\ 5.29{\times}10^{-11} meters,\ n = 1, 2, 3, ...$$

$$E_{Z,n} = -\frac{Z^2}{n^2}13.6eV,\ n = 1, 2, 3, ...$$

$$\langle\rho\rangle = \frac{E_{Z,n}}{c^2\frac{4}{3}\pi r^3_{Z,n}}.$$

TABLE II: This table compares the derived "density" of a given energy state n, with $Z = 1$ to the Casimir density for a cavity with a separation distance of $2r_n$.

n	$radius(m)$	$\rho\left(kg/m^3\right)$	$Casimir\left(kg/m^3\right)$[a]	$Ratio$[b]
1	5.29×10^{-11}	3.91×10^{-5}	1.16×10^{-4}	2.96
2	2.11×10^{-10}	1.53×10^{-7}	4.51×10^{-7}	2.96
3	4.76×10^{-10}	5.95×10^{-9}	1.76×10^{-8}	2.96
4	8.46×10^{-10}	5.96×10^{-10}	1.76×10^{-9}	2.96
5	1.32×10^{-9}	1.00×10^{-10}	2.96×10^{-10}	2.96
6	1.90×10^{-9}	2.33×10^{-11}	6.88×10^{-11}	2.96
7	2.59×10^{-9}	6.77×10^{-12}	2.00×10^{-11}	2.96

[a] This is the Casimir force per unit area multiplied by $1/c^2$.
[b] This ratio is the Casimir column value divided by the ρ column value

Friedmann equation:

$$\frac{\ddot{a}}{a} = -\frac{4\pi G}{3}\left(\rho c^2 + 3P\right)$$

$$\langle\rho\rangle = \frac{E_{Z,n}}{c^2 \frac{4}{3}\pi r_{Z,n}^3} = \frac{1}{3c^2}\frac{\hbar c \pi^2}{240 d^4}$$

$$P < -\rho c^2/3$$

$$w \sim -1/3$$

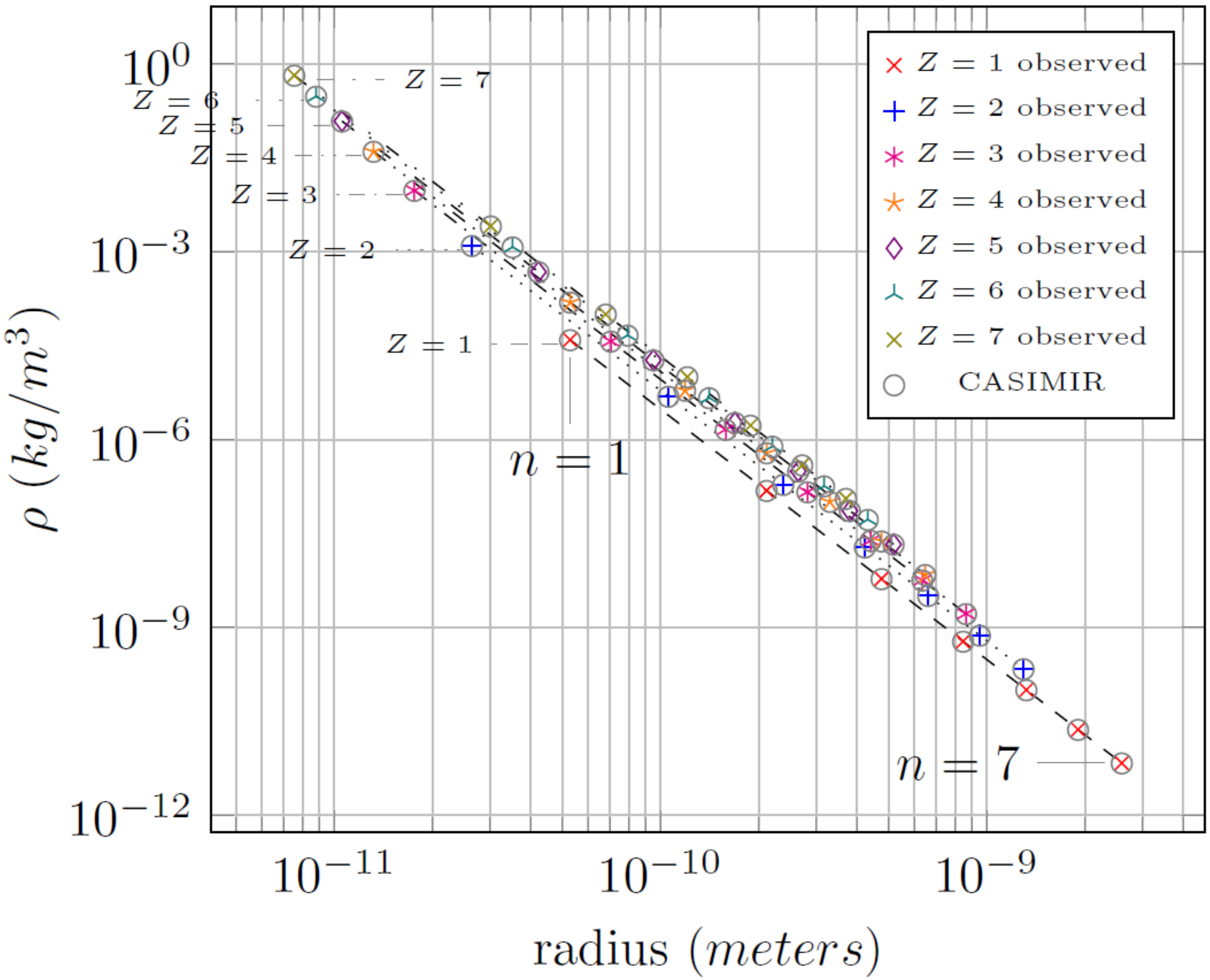

$\rho\ (kg/m^3)$
radius $(meters)$
10^{0}
10^{-3}
10^{-6}
10^{-9}
10^{-12}
10^{-11}
10^{-10}
10^{-9}
$Z = 7$
$Z = 6$
$Z = 5$
$Z = 4$
$Z = 3$
$Z = 2$
$Z = 1$
$n = 1$
$n = 7$
$Z = 1$ observed
$Z = 2$ observed
$Z = 3$ observed
$Z = 4$ observed
$Z = 5$ observed
$Z = 6$ observed
$Z = 7$ observed
CASIMIR

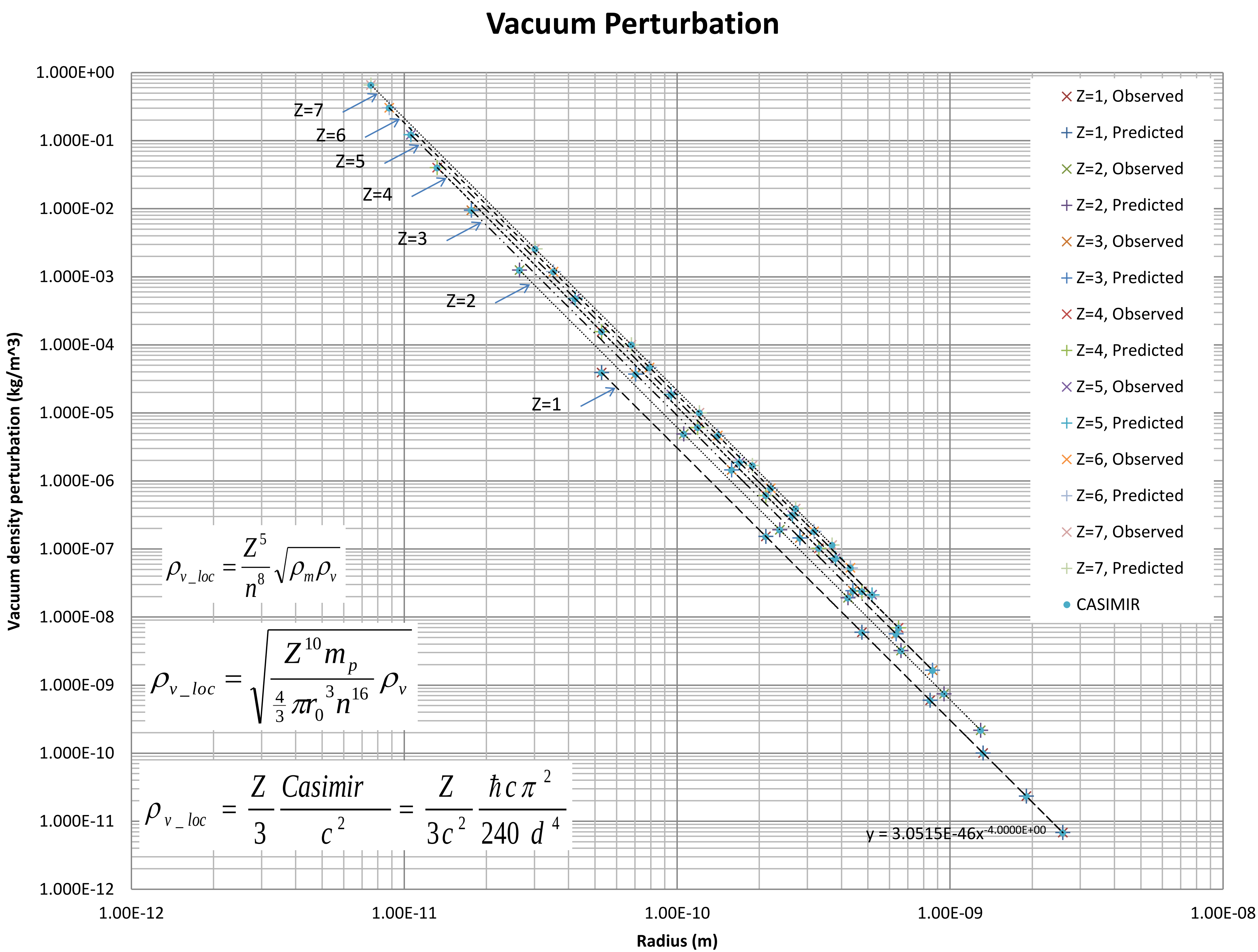
Vacuum Perturbation
Vacuum density perturbation (kg/m^3)
1.000E+00
1.000E-01
1.000E-02
1.000E-03
1.000E-04
1.000E-05
1.000E-06
1.000E-07
1.000E-08
1.000E-09
1.000E-10
1.000E-11
1.000E-12
1.00E-12
1.00E-11
1.00E-10
1.00E-09
1.00E-08
Radius (m)
Z=7
Z=6
Z=5
Z=4
Z=3
Z=2
Z=1
Z=1, Observed
Z=1, Predicted
Z=2, Observed
Z=2, Predicted
Z=3, Observed
Z=3, Predicted
Z=4, Observed
Z=4, Predicted
Z=5, Observed
Z=5, Predicted
Z=6, Observed
Z=6, Predicted
Z=7, Observed
Z=7, Predicted
CASIMIR
$\rho_{v\_loc} = \frac{Z^5}{n^8}\sqrt{\rho_m \rho_v}$
$\rho_{v\_loc} = \sqrt{\frac{Z^{10} m_p}{\frac{4}{3}\pi r_0^3 n^{16}} \rho_v}$
$\rho_{v\_loc} = \frac{Z}{3}\frac{Casimir}{c^2} = \frac{Z}{3c^2}\frac{\hbar c \pi^2}{240\ d^4}$
$y = 3.0515E\text{-}46x^{-4.0000E+00}$

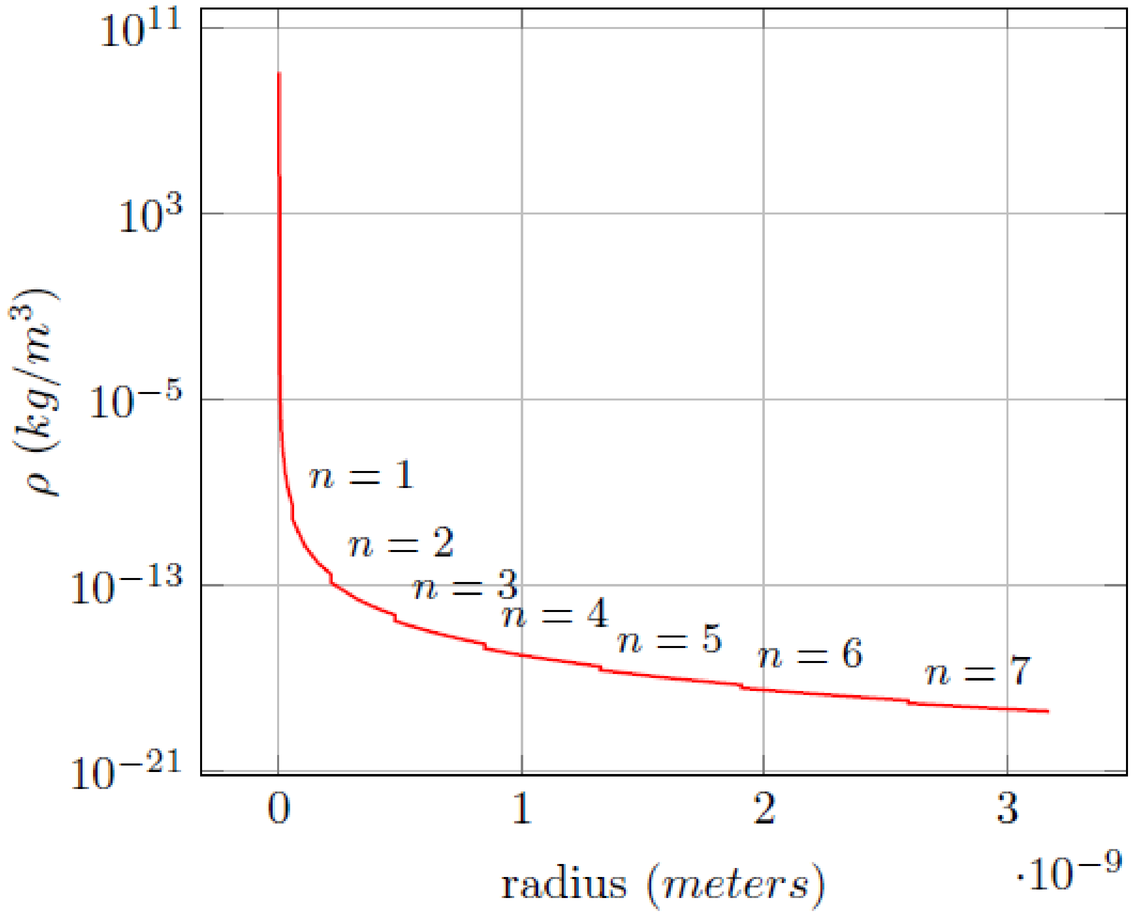
10^{11}
10^{3}
10^{-5}
10^{-13}
10^{-21}
$\rho\ (kg/m^3)$
$n = 1$
$n = 2$
$n = 3$
$n = 4$
$n = 5$
$n = 6$
$n = 7$
0
1
2
3
$\cdot 10^{-9}$
radius $(meters)$

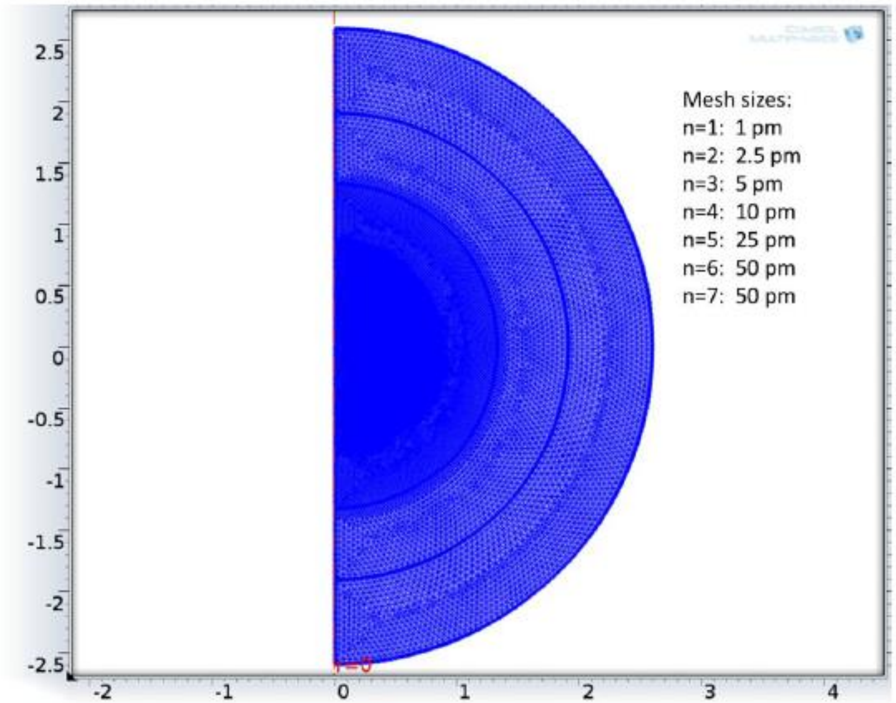

FIG. 6: COMSOL 2D axisymmetric model: element sizes for $n = 1$ to $n = 7$ is $1pm$, $2.5pm$, $5pm$, $10pm$, $25pm$, $50pm$, and $50pm$ respectively. In this figure, the mesh size is too dense to be discernable for $n = 5$ and lower. FIG. 4 shows the mesh for the $n = 1$ and $n = 2$ regions.

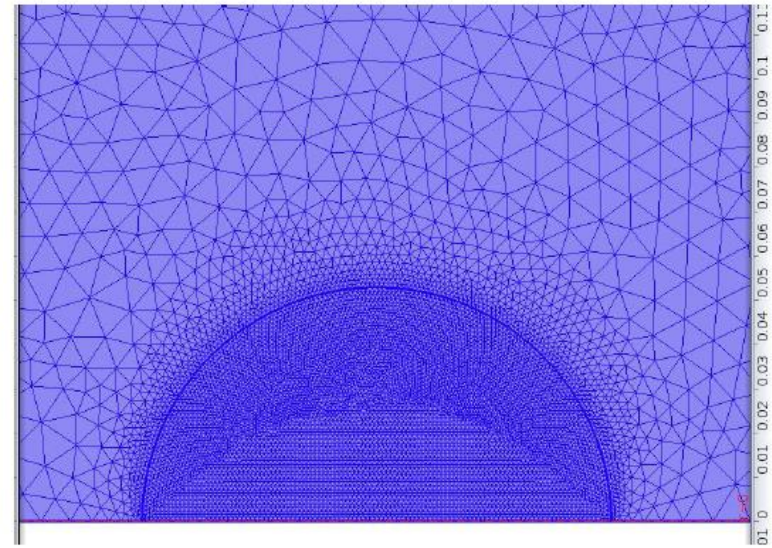

FIG. 4: Close-up of COMSOL 2D axisymmetric model.

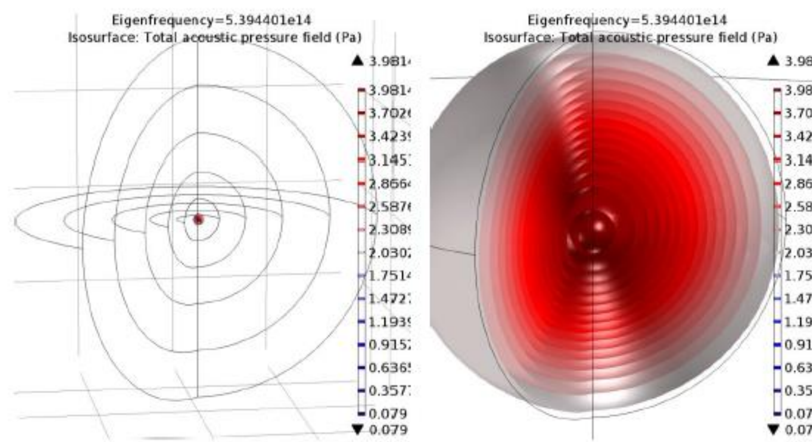

(a) Macroview (b) Microview

FIG. 5: COMSOL analysis results for $n = 1$ eigenfrequency: panel 5a shows the model out to the $n = 6$ orbital, and panel 5b shows a close-up view of the $n = 1$ solution

TABLE IV: This table shows the predicted "orbital" frequency and the COMSOL analysis eigenfrequencies for the $n = 1$ to $n = 7$ states for hydrogen.

n	*Orbital freq*[a]	*COMSOL freq*[b]	*%error*
1	6.58×10^{15}	6.25×10^{15}	−4.98
2	8.23×10^{14}	8.23×10^{14}	0.05
3	2.44×10^{14}	2.38×10^{14}	−2.48
4	1.03×10^{14}	1.01×10^{14}	−1.59
5	5.26×10^{13}	4.98×10^{13}	−5.36
6	3.05×10^{13}	3.48×10^{13}	14.28
7	1.92×10^{13}	2.13×10^{13}	11.16

[a] Orbital frequency is in Hz.
[b] COMSOL frequency is in Hz.

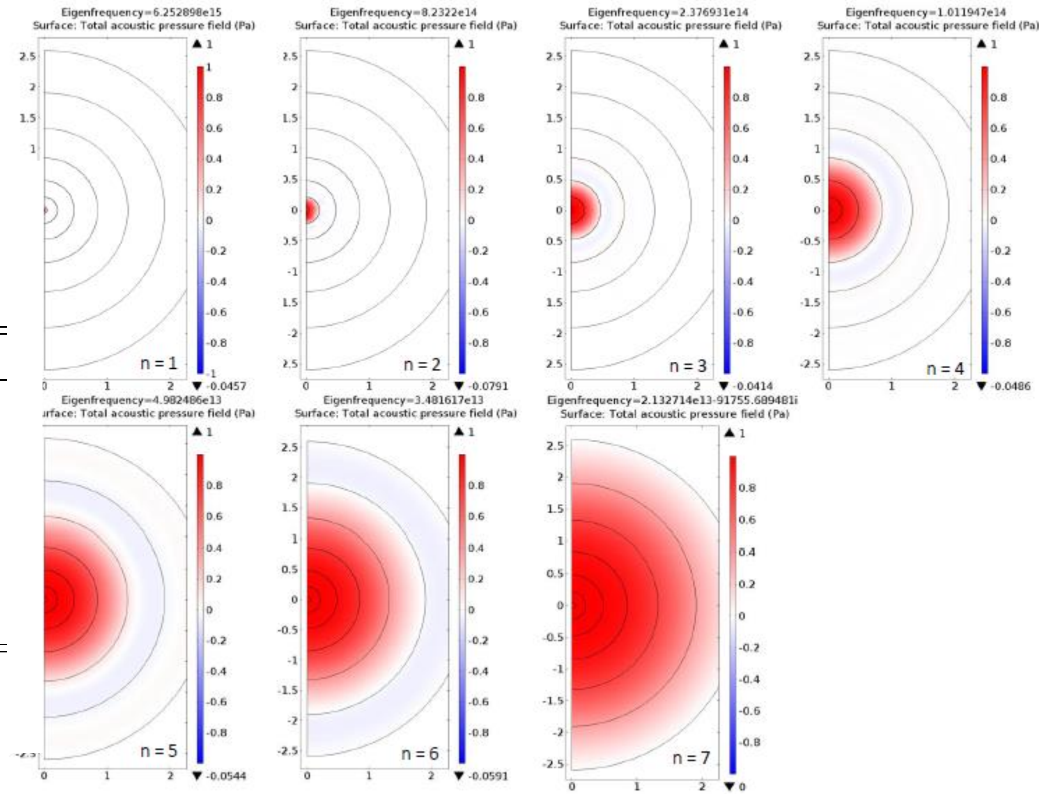

FIG. 7: COMSOL analysis results of the acoustic "natural" vacuum model The orbital shells (dark lines) can be counted, but the $n = 1$ radius is quite small as seen from the top left thumbnail that depicts the COMSOL eigenfrequency solution for that orbital.

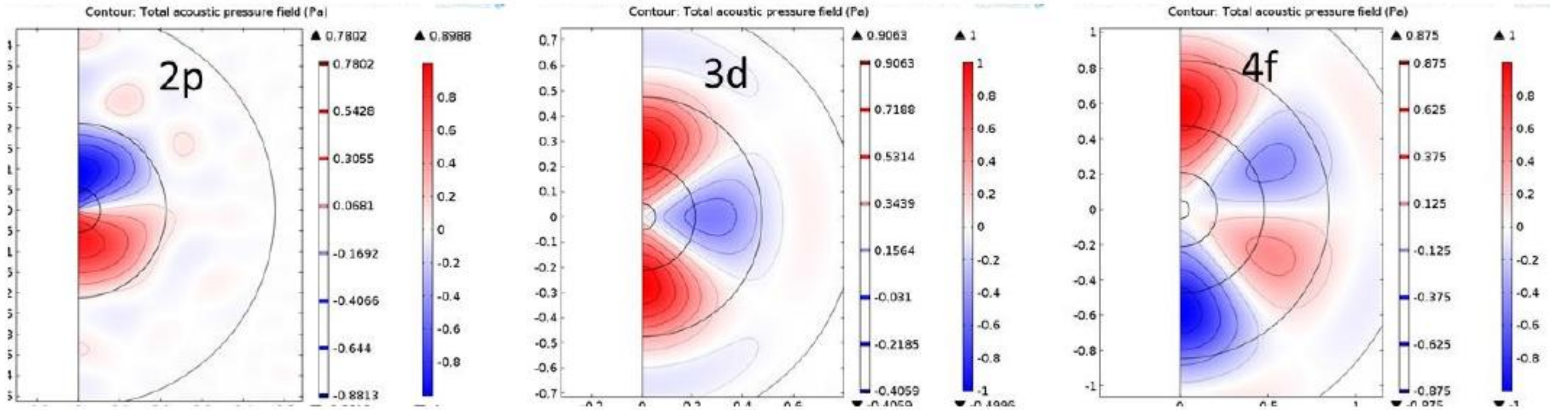

FIG. 9: 2D Axisymmetric model results that capture axisymmetric acoustic solutions like $2p$, $3d$, and $4f$ orbitals ($m = 0$).

$$i\hbar \frac{\partial \psi}{\partial t} = -\frac{\hbar^2}{2m}\frac{\partial^2 \psi}{\partial x^2} + V\psi$$

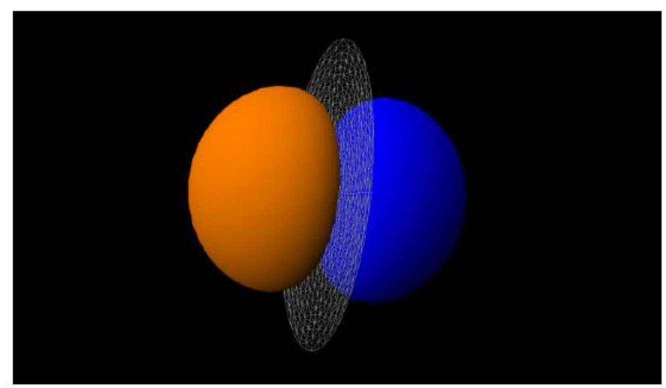

FIG. 3: Plot for the $Z = 1$, $2p$ orbital from Orbital Viewer Software.

Godspeed!